doi:10.1093/plcell/koab187

THE PLANT CELL

THE PLANT CELL 2021: 33: 3250–3271

Research Article

COMPASS functions as a module of the INO80 chromatin remodeling complex to mediate histone H3K4 methylation in Arabidopsis

Ji-Yun Shang [1,2], Yu-Jia Lu [1], Xue-Wei Cai [1], Yin-Na Su [1], Chao Feng [1], Lin Li [1], She Chen [1,3] and Xin-Jian He [1,2,3,*,†]

1 National Institute of Biological Sciences, Beijing, 102206, China
2 Graduate School of Peking Union Medical College, Beijing, China
3 Tsinghua Institute of Multidisciplinary Biomedical Research, Tsinghua University, Beijing, 100084, China

*Author for correspondence: hexinjian@nibs.ac.cn
†Senior author

These authors contributed equally (J.Y.S., Y.J.L.).

J.Y.S., Y.J.L., C.F., L.L., and S.C. performed the experiments. X.W.C. and Y.N.S. performed the bioinformatics analyses. J.Y.S., Y.J.L., and X.J.H. designed the experiments. J.Y.S. and X.J.H. wrote the manuscript.

The author responsible for distribution of materials integral to the findings presented in this article in accordance with the policy described in the Instructions for Authors (https://academic.oup.com/plcell) is: Xin-Jian He (hexinjian@nibs.ac.cn).

Abstract

In the INO80 chromatin remodeling complex, all of the accessory subunits are assembled on the following three domains of INO80: N-terminal domain (NTD), HSA domain, and ATPase domain. Although the ATPase and HSA domains and their interacting accessory subunits are known to be responsible for chromatin remodeling, it is largely unknown how the accessory subunits that interact with the INO80 NTD regulate chromatin status. Here, we identify both conserved and nonconserved accessory subunits that interact with the three domains in the INO80 complex in *Arabidopsis thaliana*. While the accessory subunits that interact with all the three INO80 domains can mediate transcriptional repression, the INO80 NTD and the accessory subunits interact with it can contribute to transcriptional activation even when the ATPase domain is absent, suggesting that INO80 has an ATPase-independent role. A subclass of the COMPASS histone H3K4 methyltransferase complexes interact with the INO80 NTD in the INO80 complex and function together with the other accessory subunits that interact with the INO80 NTD, thereby facilitating H3K4 trimethylation and transcriptional activation. This study suggests that the opposite effects of the INO80 complex on transcription are required for the balance between vegetative growth and flowering under diverse environmental conditions.

Introduction

The nucleosome, which consists of a histone octamer wrapped by 147-bp DNA, is a basic unit of chromatin. The ATP-dependent SWI2/SNF2 (SWITCH/SUCROSE NONFERMENTABLE)-type chromatin remodelers are involved in regulating the assembly, ejection, sliding, or exchanging histone variants of nucleosomes, thereby affecting the action on chromatin, including DNA replication, DNA repair, transcription, and genome stability (Luger et al., 2012; Han et al., 2015; Li et al., 2017). The SNF2 ATPase domain is conserved in the SWI/SNF2 chromatin remodelers and is responsible for ATP hydrolysis and chromatin remodeling. Based on the

Received December 14, 2020. Accepted July 11, 2021. Advance access publication July 16, 2021

IN A NUTSHELL

Background: In eukaryotic cells, the INO80 chromatin remodeling complex uses energy derived from ATP hydrolysis to change chromatin structure and the accessibility of chromatin-related proteins to DNA. The histone methyltransferase COMPASS complexes can add three methyl groups (me3) on histone 3 lysine 4 (H3K4me3) in actively transcribed genes and promote transcription. INO80 and COMPASS are two independent complexes in yeast and metazoans, with well-characterized compositions and functions. Although the biological functions of INO80 and COMPASS complexes were extensively studied in plants, the compositions of these complexes were less studied.

Question: We wanted to investigate the composition of the Arabidopsis INO80 chromatin remodeling complex and figure out how the INO80 complex regulates gene expression.

Findings: We found that the Arabidopsis INO80 complex contained ~26 conserved and non-conversed components bind to three domains of INO80: the N-terminal domain (NTD), HSA domain, and ATPase domain. In particular, a subclass of the COMPASS complex, containing the histone H3K4 methyltransferase ATX4 or ATX5, binds to the NTD of INO80 through JMJ24, a protein belonging to the H3K9me2 demethylase family. The ATX4/5-containing COMPASS complex and the other NTD-binding subunits form the NTD module, which promotes plant growth and represses flowering under short-day conditions. Furthermore, we found that the NTD module can activate gene expression by promoting H3K4me3 deposition at a subset of genes targeted by the INO80 complex in an ATPase activity-independent way.

Next steps: We will carry out chromatin immunoprecipitation and sequencing analysis to identify the target genomic loci of INO80 complex at the whole-genome level. Based on the resulting data, we will investigate how the ATPase-dependent and -independent functions of INO80 are coordinated in the regulation of gene expression, growth, and flowering time.

characteristics of domains flanking the SNF2 domain, the SWI2/SNF2 chromatin remodelers can be classified into SWI/SNF, ISWI (IMITATION SWI), CHD (Chromodomain, Helicase, and DNA binding), and INO80 (INOSITOL REQUIRING 80) families (Clapier and Cairns, 2009; Han et al., 2015). The INO80-type chromatin remodelers contain the SWI2/SNF2-RELATED 1 (SWR1) chromatin remodeler responsible for exchanging H2A for the H2A variant H2A.Z and also contain the INO80 chromatin remodeler involved in sliding nucleosomes and exchanging H2A.Z for H2A (Mizuguchi et al., 2004; Papamichos-Chronakis et al., 2011; Kapoor and Shen, 2014). The chromatin remodelers usually interact with other proteins and form multi-subunit complexes in yeast and metazoans (Clapier and Cairns, 2009; Kapoor and Shen, 2014). In plants, while the composition of the SWI/SNF, ISWI, and SWR1 chromatin remodeling complexes has been well studied (Sarnowska et al., 2016; Potok et al., 2019; Sijacic et al., 2019; Gu et al., 2020; Luo et al., 2020; Tan et al., 2020), the composition of the INO80 complex is largely unknown.

The INO80 chromatin remodeler consists of three distinct conserved domains in eukaryotes: the N-terminal domain (NTD), the HSA domain (helicase/SANT-associated domain), and the ATPase domain (Chen et al., 2011). Unlike the other types of chromatin remodelers, the INO80 chromatin remodeler has a split-ATPase domain interrupted by an inserted region (Flaus et al., 2006). In yeast and metazoans, the INO80 chromatin remodeler typically exists in a complex consisting of approximately 15 subunits (Bao and Shen, 2011; Chen et al., 2011). The chromatin remodeling activity of INO80 is dependent not only on the INO80 ATPase domain but also on INO80 accessory subunits such as RUVB-LIKE 1 (RUVBL1), RUVBL2, INO EIGHTY SUBUNIT 2 (IES2), IES6, and ACTIN-RELATED PROTEIN 5 (ARP5; Chen et al., 2013). RUVBL1 and RUVBL2 form a heterohexamer and function together with IES2, IES6, and ARP5 and assemble on the INO80 ATPase domain in the INO80 complex (Jha and Dutta, 2009; Aramayo et al., 2018). Previous biochemical and structural analyses indicate that the accessory subunits assembling on the INO80 ATPase domain are required for ATP hydrolysis as well as for nucleosome remodeling in yeast and mammals (Chen et al., 2013; Ayala et al., 2018; Eustermann et al., 2018). In addition to the accessory subunits that assemble on the INO80 ATPase domain, other accessory subunits assemble on the INO80 NTD and the HSA domain (Chen et al., 2013; Gerhold and Gasser, 2014). However, it is largely unknown how the accessory subunits that assemble on the NTD and HSA domains contribute to the function of INO80 in eukaryotes.

In *Arabidopsis thaliana*, the INO80 chromatin remodeler is required for DNA repair, plant development, floral phase transition, and photomorphogenesis (Fritsch et al., 2004; Zhang et al., 2015a; Wang et al., 2019; Yang et al., 2020). By affinity purification in combination with mass spectrometry (AP–MS), ARP5, EEN (yeast IES6 ortholog), and RVB1/2 (RIN1/2) were identified as conserved INO80 accessory subunits (Kang et al., 2019; Zander et al., 2019). ARP5 functions together with INO80 in regulating plant growth and development (Kang et al., 2019). The INO80 complex can function cooperatively with REF6 to regulate ethylene responses

(Zander et al., 2019). Unlike ARP5 and IES6, which act as subunits exclusively in the INO80 complex, RVB1/2 can also act as subunits of the SWR1 complex (Aslam et al., 2019; Potok et al., 2019; Sijacic et al., 2019; Luo et al., 2020). The sharing of RVB1/2 by the INO80 and SWR1 complexes is conserved in yeast and metazoans (Clapier and Cairns, 2009). Except for ARP5, IES6, and RVB1/2, other subunits of the INO80 complex have not been reported in Arabidopsis. Therefore, the composition and function of the INO80 complex remain to be investigated.

Histone methylation on lysine residues is associated with transcriptional activation or repression and is catalyzed by a family of SET domain-containing histone methyltransferases in eukaryotes (Shilatifard, 2008; Thorstensen et al., 2011). Trithorax-type histone H3K4 methyltransferases, which belong to a subfamily of the SET domain-containing histone methyltransferases, typically exist within multi-subunit complex of proteins associated with Set1 (COMPASS) complexes and act as master regulators of transcription in yeast and metazoans (Smith et al., 2011; Fromm and Avramova, 2014). In Arabidopsis, there are five conserved Trithorax-type histone H3K4 methyltransferases, ARABIDOPSIS TRITHORAX 1–5 (ATX1–5), which can be divided into two subgroups: ATX1/2 and ATX3/4/5 (Alvarez-Venegas and Avramova, 2012). ATX1 and ATX2 are involved in the suppression of flowering by promoting H3K4 trimethylation and transcriptional activation of the flowering repressor gene *FLOWERING LOCUS C* (*FLC*; Pien et al., 2008). In addition, ATX1 was also reported to be required for abscisic acid response and dehydration tolerance (Ding et al., 2011). In the ATX3/4/5 group, ATX4 is closely related to ATX5 and is distantly related to ATX3 (Alvarez-Venegas and Avramova, 2012). ATX3, ATX4, and ATX5 function redundantly in vegetative and reproductive development (Chen et al., 2017). ATX4 and ATX5 were also reported to be required for abscisic acid and dehydration stress responses (Liu et al., 2018). ATX1 interacts with the conserved COMPASS accessory subunits WDR5A, RBL, and TRO (ASH2R), and forms a COMPASS-like complex involved in the regulation of flowering time and development (Jiang et al., 2011). The interaction of ATX3 and ATX4 with WDR5A has also been demonstrated (Jiang et al., 2011). Although several conserved COMPASS subunits have been identified in Arabidopsis, it remains to be determined whether the Arabidopsis COMPASS complex contains additional subunits.

In this study, we identified three JmjC domain-containing histone demethylases, JMJ24, JMJ26, and JMJ28, as additional subunits of the Arabidopsis COMPASS complexes that contain ATX4 and ATX5 (ATX4/5), ATX3, and ATX1/2, respectively. We also identified the conserved and nonconserved subunits of the Arabidopsis INO80 complexes. The ATX4/5-containing COMPASS complex interacts with the INO80 NTD and acts as a module of the INO80 complex in Arabidopsis. JMJ24 is a bridge protein that is responsible for assembling the COMPASS module on the INO80 NTD. Furthermore, we demonstrated that INO80 has both ATPase-dependent and ATPase-independent roles. The accessory subunits associated with the NTD including the ATX4/5-containing COMPASS complex are involved in transcriptional activation via histone H3K4 trimethylation in an ATPase-independent manner.

Results

A subclass of the COMPASS complex acts as a module of the INO80 chromatin remodeling complex in Arabidopsis

The conserved chromatin remodeler INO80 is involved in DNA repair, histone modifications, and the regulation of development in Arabidopsis (Fritsch et al., 2004; Zhang et al., 2015a; Zander et al., 2019; Yang et al., 2020). The INO80 orthologs typically associate with accessory subunits and form multi-subunit complexes in eukaryotes. However, while the composition of the INO80 complex is well known in yeast and metazoans (Bao and Shen, 2011; Chen et al., 2013), it is largely unknown in plants. We generated transgenic plants harboring a native promoter-driven *INO80-Flag* fusion transgene and carried out AP–MS to identify the composition of the INO80 complex in Arabidopsis. AP–MS identified a number of conserved INO80 accessory subunits; these conserved subunits were named according to the names of their orthologs in other eukaryotes (Figure 1, A and B; Supplemental Data set S1). This finding suggests that the INO80 complex components are conserved among plants and other eukaryotes.

Our AP–MS data also showed that two closely related Trithorax-type histone H3K4 methyltransferases, ATX4/5, but not their homologs, ATX1, ATX2, and ATX3 (ATX1/2/3), were co-purified with INO80 (Figure 1, A and B). The interaction of ATX4/5 with INO80 was demonstrated by co-immunoprecipitation (co-IP; Figure 1C). In the ATX1-containing COMPASS complex, ATX1 is known to interact with the accessory subunits TRO/ASH2R, WDR5A, and RBL (Jiang et al., 2011). We found that, in addition to ATX4/5, all of the accessory subunits can also be co-purified with INO80 (Figure 1, A and B). Furthermore, ATX4/5, TRO, WDR5A, and RBL can also be co-purified with the INO80 accessory subunits tested (UCH1, UCH2, NFRKB1, NFRKB2, INB1, INB2A, INB2B, INB3, YY1, ARP9, IES2A, IES2B, ARP5, EEN, RIN1, and RIN2) (Figure 1, A and B; Supplemental Data set S1), suggesting that the ATX4/5-containing COMPASS complex can interact with the INO80 complex. By using transgenic plants expressing ATX1, ATX2, ATX3, ATX4, and ATX5 tagged by Flag epitope, we performed AP-MS and found that the INO80 complex was co-purified with ATX4 and ATX5 but not with the ATX1, ATX2, or ATX3 (Figure 1, A and B; Supplemental Data set S1). These results demonstrate that the ATX4/5-containing COMPASS complex but not the ATX1/2/3-containing COMPASS complex functions as a module of the INO80 complex. The following four previously uncharacterized proteins were also shown to act as INO80 subunits: INO80-binding protein 1 (INB1), the two

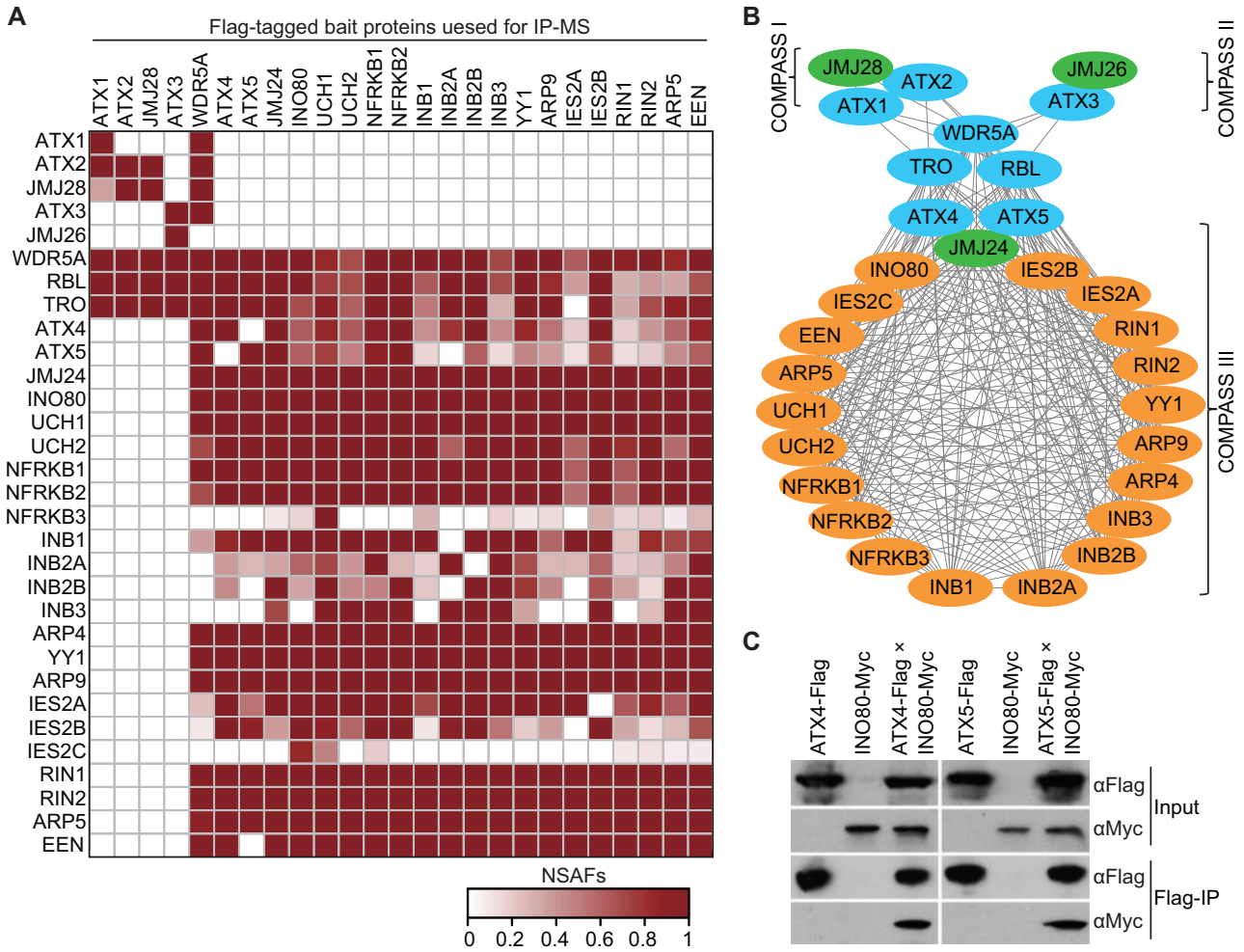

Figure 1 Identification of a subclass of COMPASS as a module of the INO80 complex. A, Heatmap visualization of the components identified in the INO80 complex and COMPASS complexes. The color gradient illustrates the NSAFs. B, The protein–protein interaction networks generated with Cytoscape by using mass spectrometric data. Edges show the interactions identified by AP–MS. Conserved subunits of COMPASS complexes are shown in cyan; three JmjC domain-containing COMPASS subunits are shown in green; all other INO80 subunits are shown in orange. C, Co-IP of INO80-Myc with ATX4-Flag and ATX5-Flag. Plants carrying *ATX4-Flag* or *ATX5-Flag* and *INO80-Myc* transgenes were used for co-IP.

closely related homologs INB2A and INB2B (INB2A/2B), and INB3 (Figure 1, A and B). Given that INB1, INB2A/2B, and INB3 are conserved in plants but not in other eukaryotes (Supplemental Figure S1), these proteins apparently represent plant-specific subunits of the INO80 complex.

Interestingly, our AP–MS data indicated that three putative JmjC domain-containing histone demethylases, JMJ28, JMJ26, and JMJ24, can interact with ATX1/2, ATX3, and ATX4/5, respectively (Figure 1, A and B). The interaction of JMJ24 with ATX4/5 was demonstrated by co-IP (Supplemental Figure S2). Moreover, JMJ24 and JMJ28 can also interact with all of the conserved COMPASS accessory components, that is, TRO, WDR5A, and RBL (Figure 1, A and B), strongly suggesting that the JmjC domain-containing proteins can act as components of the COMPASS complexes in Arabidopsis. Consistent with the finding that the ATX4/5-containing COMPASS but not the ATX1/2/3-containing COMPASS is present in the INO80 complex, our AP–MS assay identified JMJ24 but not JMJ26 and JMJ28 in the INO80 complex (Figure 1, A and B; Supplemental Data set S1). Unlike JMJ26 and JMJ28, which can only interact with the COMPASS components, JMJ24 has evolved the additional ability to interact with the INO80 complex.

The ATX4/5-containing COMPASS complex has a similar biological function with a subset of INO80 accessory components

Researchers previously reported that loss-of-function mutations in INO80 and in the conserved INO80 accessory subunit ARP5 resulted in retarded plant growth (Kandasamy et al., 2009; Zhang et al., 2015a; Kang et al., 2019). We obtained mutants of conserved components in the INO80 complex, which included T-DNA insertion mutants of *INO80*, *NFRKB1/2/3*, *YY1*, *ARP9*, and *ARP5*, and the CRISPR/Cas9-induced mutants of *UCH1/2* and *EEN* (Supplemental Figure S3), and found that these mutants showed obvious growth retardation under long-day (LD) conditions even though the retardation was less severe in the mutants of the INO80

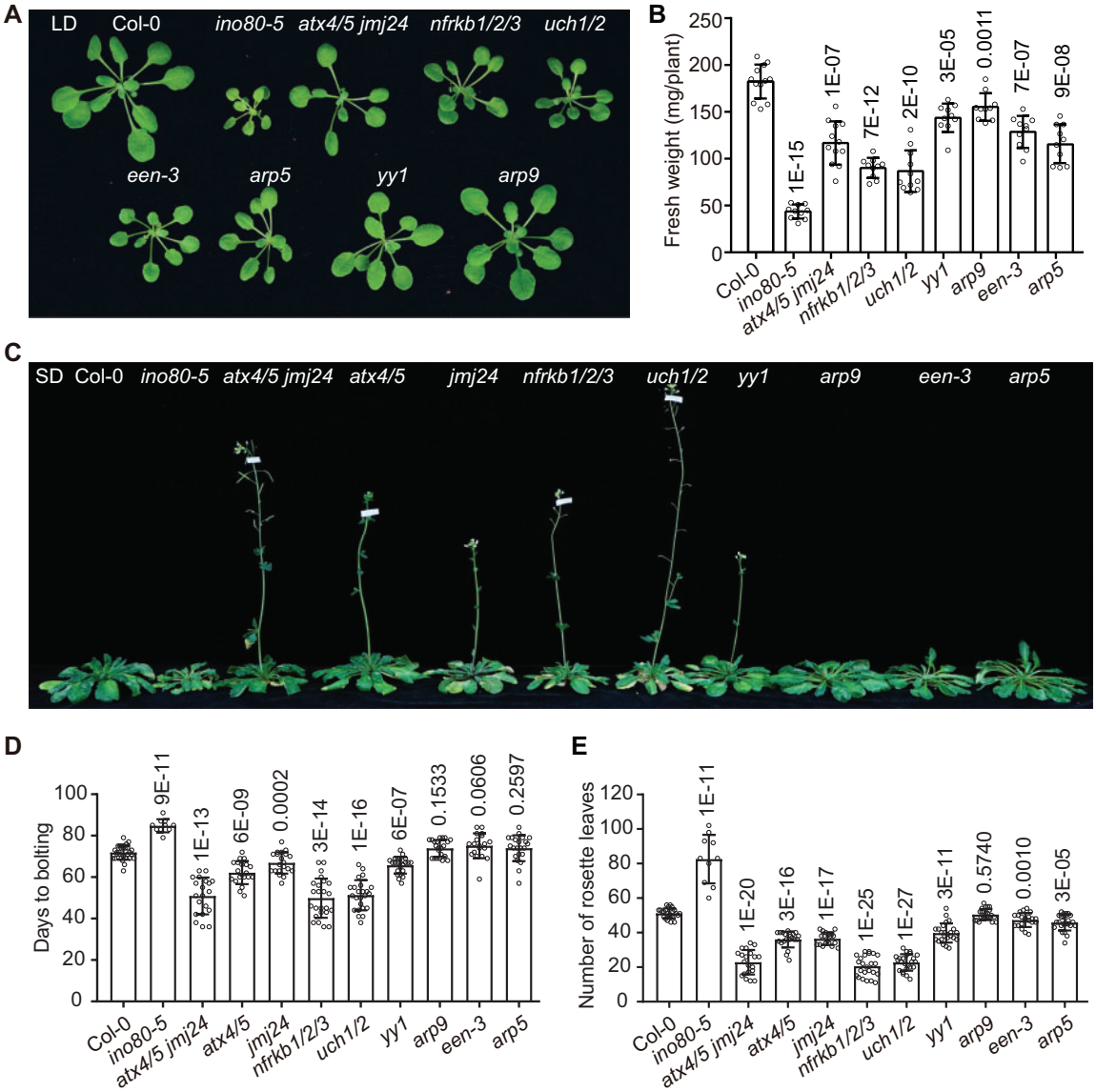

Figure 2 ATX4/5 and JMJ24 function in coordination with other subunits of the INO80 complex to regulate vegetative development and flowering time. A, Morphological phenotypes of 22-day-old WT and mutant plants grown under LD conditions. B, Fresh weight per plant was determined using at least 10 plants grown under LD conditions for 22 days. C, Morphological phenotypes of WT and mutant plants grown under SD conditions. D and E, Flowering time was measured by counting the days to bolting (D) and the number of rosette leaves at bolting (E). Values are means ± standard deviation (SD) ($n = 10–24$). *P*-values were determined by Student's *t* test.

accessory components than in the *ino80-5* mutant (Figure 2, A and B; Supplemental Figure S4). The *nfrkb1*, *nfrkb2*, and *nfrkb3* single mutants and *uch1* and *uch2* single mutants did not show obvious growth retardation or showed only slight growth retardation under LD conditions (Supplemental Figures S5 and S6). However, the growth retardation was obvious in the double or triple mutants of *NFRKB1/2/3* and in the double mutant of *UCH1/2* (Supplemental Figures S4–S6). The growth retardation of *nfrkb1/2* and *uch1/2* mutant plants was restored to wild-type (WT) or single-mutant levels by *NFRKB1/2* and *UCH1/2* transgenes, respectively (Supplemental Figures S5 and S6), suggesting that the NFRKB1/2/3 and UCH1/2 homologs function redundantly in the INO80 complexes.

Considering that the ATX4/5-containing COMPASS complex can function as a module of the INO80 complex, we investigated whether the COMPASS complex has the same biological function as the INO80 complex. While the *atx4* and *atx5* single mutants had no obvious morphological defects, the *atx4/5* double mutant showed retarded growth compared to the Col-0 WT (Supplemental Figure S7). Similarly, the *jmj24* mutant also showed retarded growth under normal light conditions (Supplemental Figure S8). We generated an *atx4/5 jmj24* triple mutant by genetic crossing and found that the growth retardation was stronger in the *atx4/5 jmj24* triple mutant than in the *atx4/5* double mutant or in *jmj24* single mutants (Figure 2, A and B; Supplemental Figure S4). These data support the inference

that the COMPASS components ATX4/5 and JMJ24 can function in the INO80 complex to regulate plant growth. To investigate whether the plant-specific subunits INB1, INB2A, INB2B, and INB3 function in plant growth regulation, we obtained the CRISPR/Cas9-mediated mutants *inb1* and *inb2a/2b* (Supplemental Figure S3) and the T-DNA insertion mutant *inb3*. However, we did not find any obvious growth retardation in these mutants (Supplemental Figure S9, A–C).

Moreover, we found that *atx4/5*, *jmj24*, and *atx4/5 jmj24* mutant plants showed significantly earlier flowering than WT plants under short-day (SD) but not LD conditions (Figure 2, C–E; Supplemental Figure S10). Given the finding that the ATX4/5-containing COMPASS complex can function as a module of the INO80 complex, the early flowering phenotype was also expected in the INO80 complex mutants. As expected, the flowering time of *nfrkb1/2/3*, *uch1/2*, and *yy1* was earlier than that of the WT under SD conditions, while the flowering time of *nfrkb1/2/3* and *uch1/2* was similar to that of the WT under LD conditions (Figure 2, C–E; Supplemental Figure S10), further supporting the inference that the COMPASS complex can regulate flowering time by functioning as a module of the INO80 complex. Although the *inb1*, *inb2a/2b*, and *inb3* mutants lacked obvious growth defects (Supplemental Figure S9, A–C), the flowering time was weakly accelerated in *inb1*, *inb2a/2b*, and *inb3* (Supplemental Figure S9, D–F), supporting the inference that the plant-specific subunits INB1, INB2A/2B, and INB3 can function as subunits of the INO80 complex to regulate flowering time. However, the flowering time of the *arp5*, *arp9*, and *een-3* mutants was similar to that of the WT under SD conditions, while the flowering time of the *ino80-5* mutant was even delayed relative to the WT under both LD and SD conditions (Figure 2, C–E; Supplemental Figure S10). The later results shown in this study will clarify why only a subset of the INO80 components (COMPASS, NFRKB1/2/3, UCH1/2, YY1, INB1, INB2A/2B, and INB3) can delay flowering.

The ATX4/5-containing COMPASS complex and a subset of INO80 accessory components interact with the INO80 NTD

In yeast and animals, the conserved INO80 chromatin remodeler not only functions as a catalytic subunit of the INO80 complex but also as a scaffold that is responsible for assembling accessory subunits of the complex; accessory subunits of the INO80 complex can interact with INO80 through three conserved domains: the NTD, HSA domain, and ATPase domain (Chen et al., 2013; Gerhold and Gasser, 2014). The HSA and ATPase domains are conserved in eukaryotes, but the NTD is divergent (Figure 3A; Supplemental Figure S11). Although the assembly of accessory subunits on INO80 has been well studied in yeast and metazoans, it is largely unknown how the accessory subunits assemble on INO80 in plants. We, therefore, generated transgenic plants expressing a series of truncated INO80 proteins (1–335 aa, 1–550 aa, 335–1540 aa, and 550–1540 aa) tagged by the Flag epitope and then performed AP–MS to determine how the truncations affect the interaction of INO80 with the accessory components (Figure 3A; Supplemental Figure S12). The AP–MS result indicated that NFRKB1/2/3 and UCH1/2 interact with the NTD; IES2A/B/C, RIN1/2, EEN, and ARP5 interact with the ATPase domain; and ARP9 interacts with the HSA domain (Figure 3B; Supplemental Data set S1). These results suggest that the interaction domains of INO80 with these conserved accessory subunits are comparable with those in humans (Chen et al., 2013). The ARP4 and YY1 orthologs exclusively interact with the INO80 HSA domain in humans (Chen et al., 2013). In Arabidopsis, however, both the HSA domain and NTD are sufficient for interacting with ARP4 and YY1 (Figure 3B), suggesting that the interaction domain of INO80 with ARP4 and YY1 in Arabidopsis is different from that in humans. In addition to the conserved INO80 subunits, we determined that the plant-specific subunits, including the ATX4/5-containing COMPASS complex, INB1, INB2A/2B, and INB3, exclusively interact with the INO80 NTD in the INO80 complex (Figure 3B; Supplemental Data set S1). These results suggest that all of the newly identified plant-specific subunits function together with a subset of conserved subunits and interact with the INO80 NTD in the INO80 complex.

To investigate how the different COMPASS subunits interact with INO80, we introduced the full-length *INO80-Flag* fusion transgene into the *atx4/5* and *jmj24* mutants and conducted AP–MS in order to determine whether the *atx4/5* and *jmj24* mutations affect the interaction of the COMPASS components with INO80. The AP–MS result indicated that the *jmj24* mutation disrupted the interaction of INO80 with all of the COMPASS components, and that the *atx4/5* mutation disrupted the interaction of INO80 with TRO, WDR5A, and RBL but not with JMJ24 (Figure 3B; Supplemental Data set S1). We further generated *JMJ24-Flag* transgenic plants in the *atx4/5* mutant background and performed AP–MS. Unsurprisingly, the loss-of-function mutation of ATX4 and ATX5 perturbed the interaction of JMJ24 with the COMPASS complex but not with INO80 complex (Figure 3B; Supplemental Data set S1), suggesting that JMJ24 functions as a bridge protein between INO80 and all of the other COMPASS components, whereas ATX4/5 is responsible for the interaction of JMJ24 with the remaining COMPASS components (TRO, WDR5A, and RBL). To verify whether JMJ24 directly interacts with INO80, we purified full-length JMJ24 and truncated INO80 (1–550 aa) proteins and performed an in vitro pull-down assay. The result showed a direct interaction between JMJ24 and the N-terminal region of INO80 (Figure 3C). We carried out yeast two-hybrid (Y2H) analysis to identify the ATX4/5–JMJ24 interaction domains and found that the second PHD domain of ATX4/5 can interact with the two zinc finger domains of JMJ24 (Figure 3D; Supplemental Figure S13). These results suggest that the ATX4/5–JMJ24–INO80 interaction is necessary for integrating all of the COMPASS components into the INO80 complex (Figure 3D).

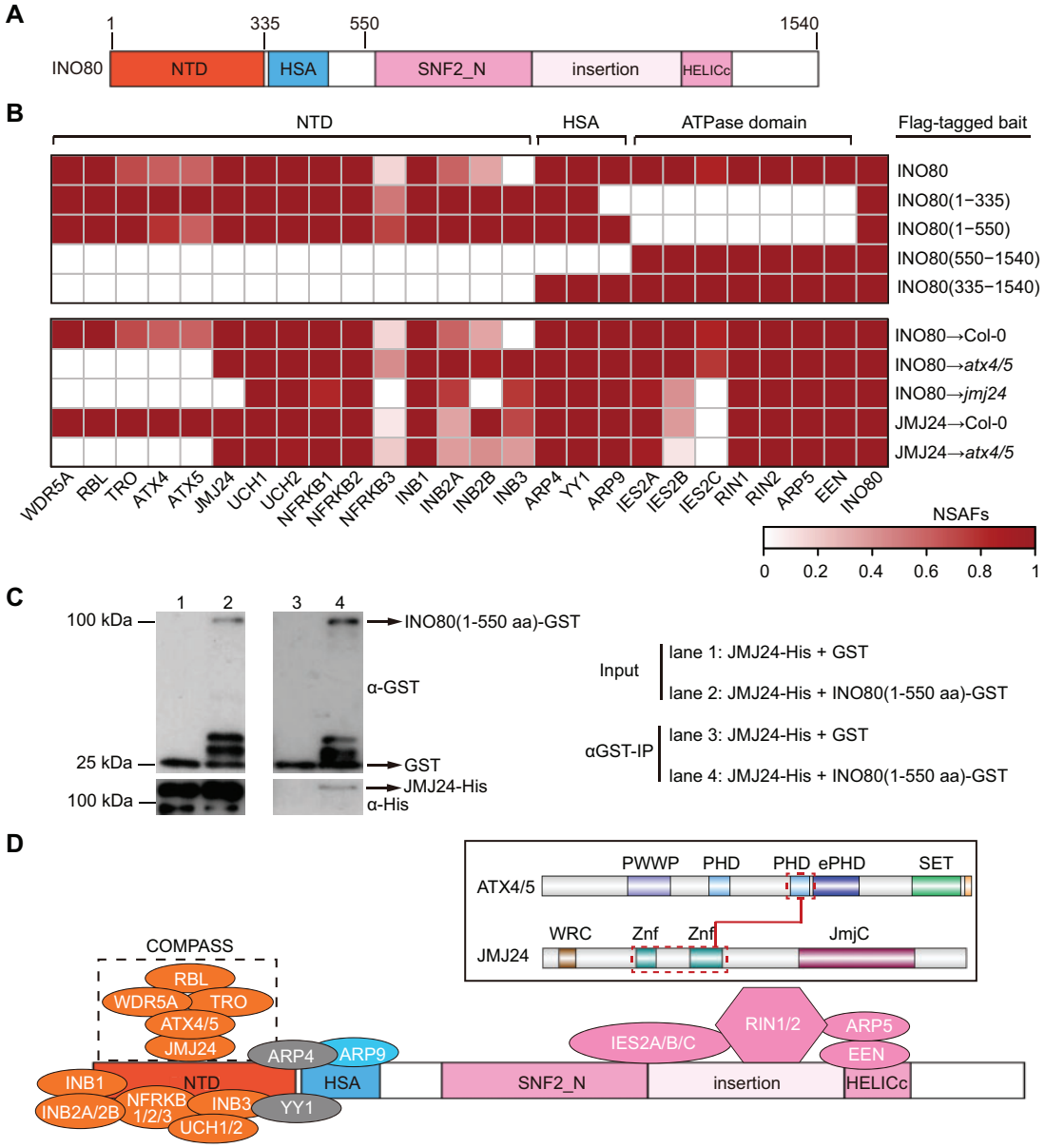

Figure 3 The modular architecture of the Arabidopsis INO80 complex. A, Schematic diagram illustrating the domain architecture of the INO80 protein. The protein length and positions of domains are drawn approximately to scale. The numbers indicate the positions of amino acids used to express the truncated INO80-Flag. B, Heatmap displaying subunits assembled at the NTD, HSA, and ATPase domains of INO80. Color bar represents the NSAFs. Plants used in AP–MS include full-length and truncated *INO80-Flag* transgenic plants in the WT background and *INO80-Flag* and *JMJ24-Flag* transgenic plants in the WT and indicated mutant backgrounds. C, The interaction between NTD of INO80 and JMJ24 was detected by a GST-pull down assay. The truncated INO80(1–550 aa) and full-length JMJ24 were used for the interaction assay. D, The architecture of the INO80 complex as determined by AP–MS, GST-pull down and Y2H analyses. The interaction between the second PHD domain of ATX4/5 and two zinc finger domains of JMJ24 as determined by Y2H are shown in the inserted chart.

Because the ATX4/5-containing COMPASS complex functions as a module of the INO80 complex, the interaction between ATX4/5-containing COMPASS complex and INO80 might be important for the function of COMPASS complex. We introduced the *ATX4-Flag* and *ATX5-Flag* transgenes into the *ino80-5* mutant plants and found that the *ino80-5* mutation resulted in remarkably reduced levels of ATX4/5-Flag proteins as determined by immunoblotting, even though it did not obviously affect the transcript levels of *ATX4/5-Flag* as determined by reverse transcription followed by quantitative PCR (RT-qPCR) (Figure 4, A and C). Furthermore, we introduced *ATX4-Flag* and *ATX5-Flag* transgenes into the *jmj24* mutant plants and determined the effect of *jmj24* on the protein levels of ATX4/5-Flag. The result showed that, although the *jmj24* mutation did not reduce the transcript levels of *ATX4/5-Flag*, it markedly reduced the protein levels of ATX4/5-Flag (Figure 4, B and D). We found that mutations of *ATX4* and *ATX5*, however, did not obviously affect the protein levels of JMJ24-Flag and INO80-Flag (Supplemental Figure S14). These results indicate

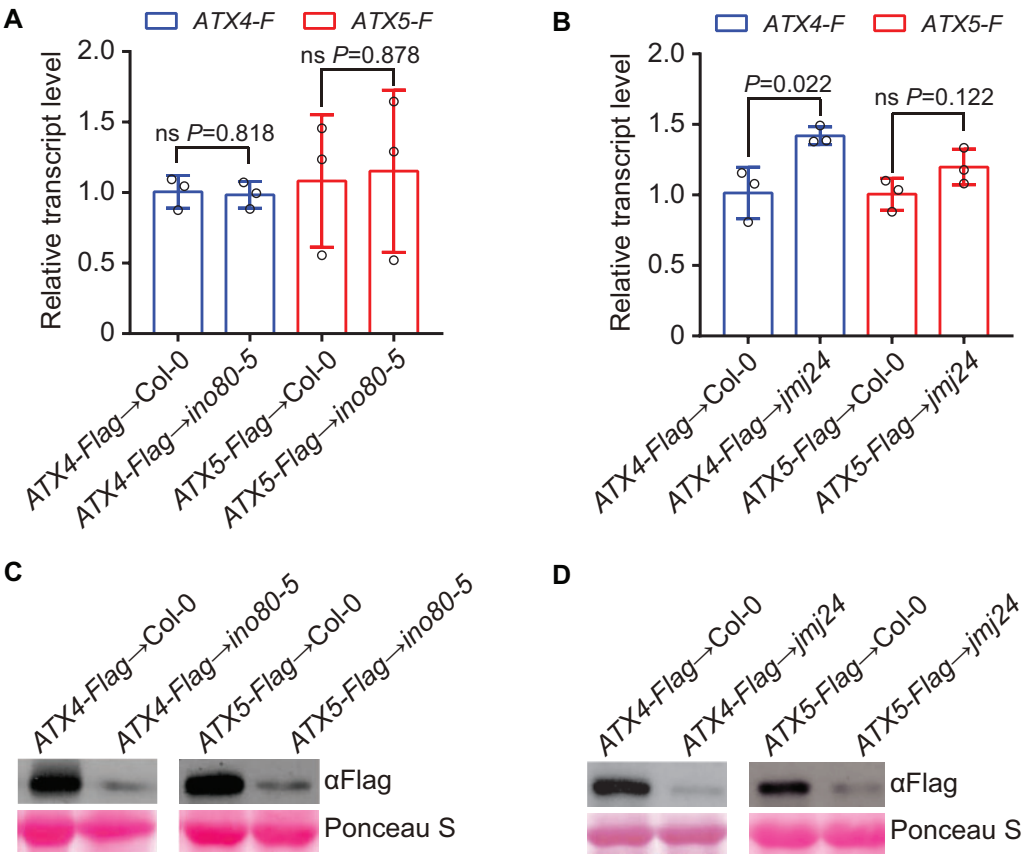

Figure 4 INO80 and JMJ24 are required for maintenance of normal protein levels of ATX4 and ATX5. A and B, The transcript levels of *ATX4-Flag* and *ATX5-Flag* in the Col-0, *ino80-5* (A), and *jmj24* (B) background were determined by RT-qPCR. Values are presented as means ± SD from three biological replicates. *P*-values were calculated by Student's *t* test. C and D, Immunoblot analysis showing the protein levels of ATX4-Flag and ATX5-Flag in the Col-0, *ino80-5* (C), and *jmj24* (D) background determined by anti-Flag antibody. The loading control was visualized by Ponceau S staining.

that the connection between ATX4/5-containing COMPASS complex and INO80 mediated by JMJ24 in the INO80 complex is essential for maintenance of normal protein levels of ATX4/5, strongly suggesting that ATX4/5-containing COMPASS complex functions as a module of the INO80 complex in Arabidopsis.

JMJ24 is a JmjC domain-containing protein belonging to KDM3/JHDM2 family (Lu et al., 2008; Saze et al., 2008). The JHDM2 family proteins have been shown to be responsible for demethylation at the histone H3K9 site (Klose et al., 2006; Yamane et al., 2006; Hyun et al., 2017). While the Arabidopsis JHDM2 family protein INCREASE IN BONSAI METHYLATION 1 (IBM1) contains a conserved JmjC domain and have an active histone H3K9 demethylase activity (Saze et al., 2008; Inagaki et al., 2010), JMJ24 contains substitutions at conserved residues in the putative JmjC domain and has been shown to be an inactive histone demethylase as determined by an in vitro assay (Lu et al., 2008; Deng et al., 2015; Kabelitz et al., 2016; Figure 5A). However, it has been shown that JMJ24 is required for maintenance of the basal transcription levels of several transposable elements through counteracting H3K9me2 (Deng et al., 2015; Kabelitz et al., 2016). Therefore, the possibility of in vivo histone demethylase activity of JMJ24 cannot be completely excluded. It was reported that a point mutation of Fe(II)-binding amino acid H1120 in JHDM2A can abolish the enzymatic activity of JHDM2A both in vitro and in vivo (Yamane et al., 2006). To further determine whether the putative histone demethylase activity is necessary for the biological function of JMJ24, we generated *JMJ24* transgenic plants harboring a point mutation (H665A) due to the conservation between H665 in JMJ24 and H1120 in JHDM2A (Figure 5A). If JMJ24 functions as an active histone demethylase, the H665A mutation was expected to disrupt its biological function. We found that the flowering time phenotype of the *jmj24* mutant was restored by the mutated *JMJ24* transgene as well as by the WT transgene (Figure 5, B–D). This strongly supports the notion that JMJ24 can function in the INO80 complex in a histone demethylase-independent manner.

The INO80 NTD has an ATPase-independent role by interacting with a subset of INO80 accessory components

Our AP–MS results demonstrate that, in the INO80 complex, the COMPASS module, INB1/2A/2B/3, NFRKB1/2/3,

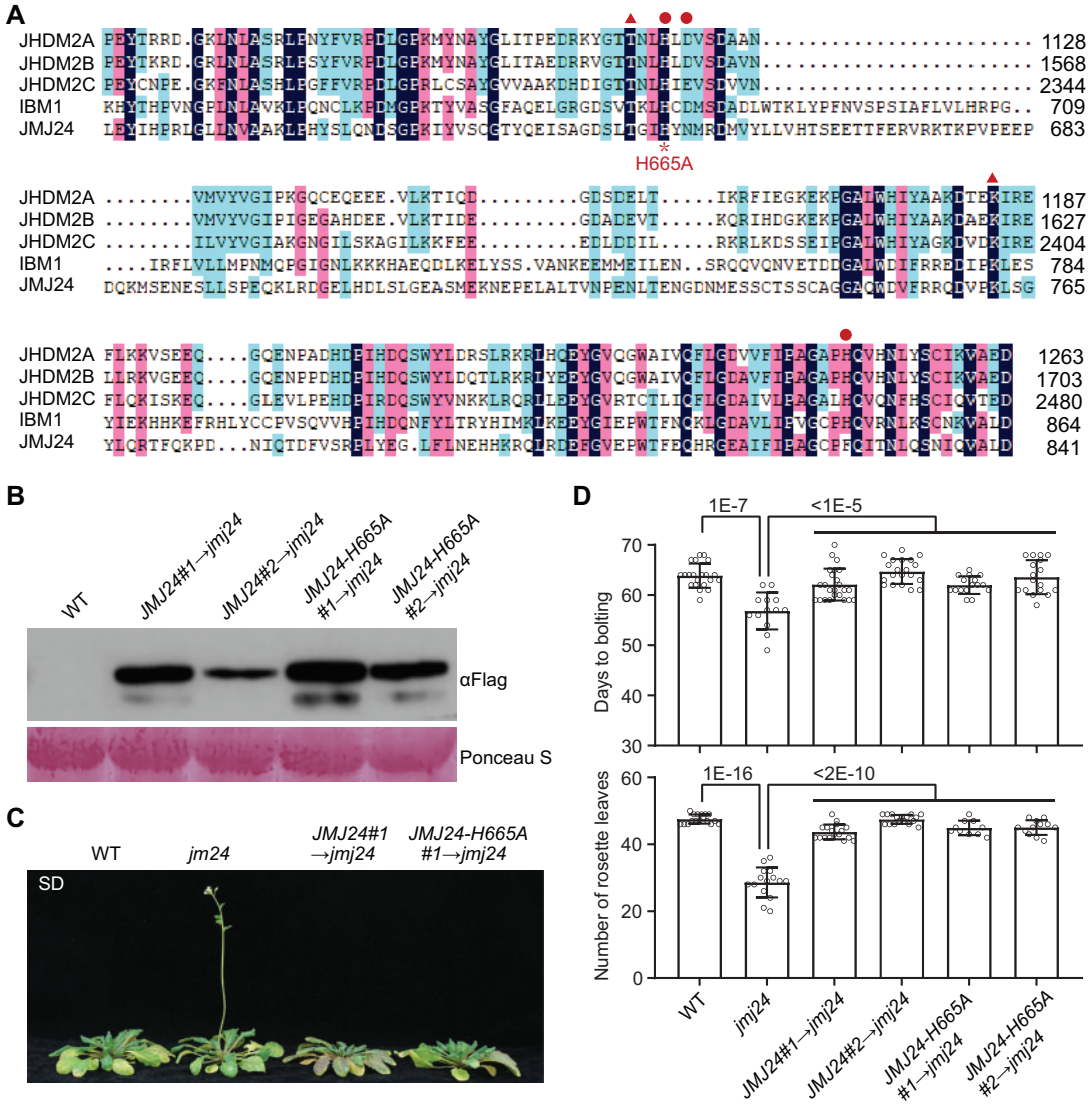

Figure 5 JMJ24 regulates flowering time in a histone demethylase activity independent way. A, Multiple sequence alignment of the JmjC domains in the Arabidopsis JMJ24 and IBM1 and in the closely related human JmjC domain-containing histone methyltransferases including JHDM2A, JHDM2B, and JHDM2C. Identical, highly conserved, and intermediately conserved residues are highlighted by dark blue, pink, and cyan, respectively. Conserved Fe(II) binding sites and α-ketoglutarate binding sites are indicated with filled circles and arrowheads, respectively. An asterisk denotes the position of the H665A point mutation generated in this study. B, Expression levels of JMJ24-Flag or JMJ24-H665A-Flag in the *jmj24* mutant background as determined by immunoblotting. Results are shown for two independent transgenic lines. C, Flowering time phenotypes of the WT, *jmj24*, and of the *jmj24* mutants expressing *JMJ24* or *JMJ24-H665A* transgenes grown under SD conditions. D, Number of days to bolting (upper) and number of rosette leaves at bolting (lower) in the indicated genotypes. Values are means ± SD from at least 10 plants per genotype. *P*-values were determined by Student's *t* test.

and UCH1/2 interact with the INO80 NTD; YY1 and ARP4 interact with both the NTD and HSA domains; and the remaining subunits interact with the HSA and ATPase domains (Figure 3). By comparing the AP–MS results and the phenotypic analyses of the INO80 complex mutants, we found that, under SD conditions, an early flowering phenotype was observed in mutants of the NTD-interacting subunits, which include *atx4/5 jmj24*, *nfrkb1/2/3*, *uch1/2*, and *yy1*, but not in the mutants of the subunits assembled on the HSA and ATPase domains, even though all of the INO80 complex mutants tested are all necessary for plant growth (Figure 2; Supplemental Figure S4). Therefore, suppression of flowering under SD conditions can be exclusively attributed to the accessory subunits assembled on the INO80 NTD.

To investigate whether the NTD, HSA, and ATPase domains of INO80 differentially regulate the biological function of INO80, we transformed a series of truncated *INO80* transgenes that encode INO80 (1–335 aa), INO80 (1–550 aa), INO80 (335–1540 aa), and INO80 (550–1540 aa) into the *ino80-5* mutant for complementation testing. As expected, the full-length INO80 completely complemented the defects in the *ino80-5* mutant (Figure 6, A and B; Supplemental Figure S15). Unexpectedly, the growth retardation of the *ino80-5* mutant was partially restored by the

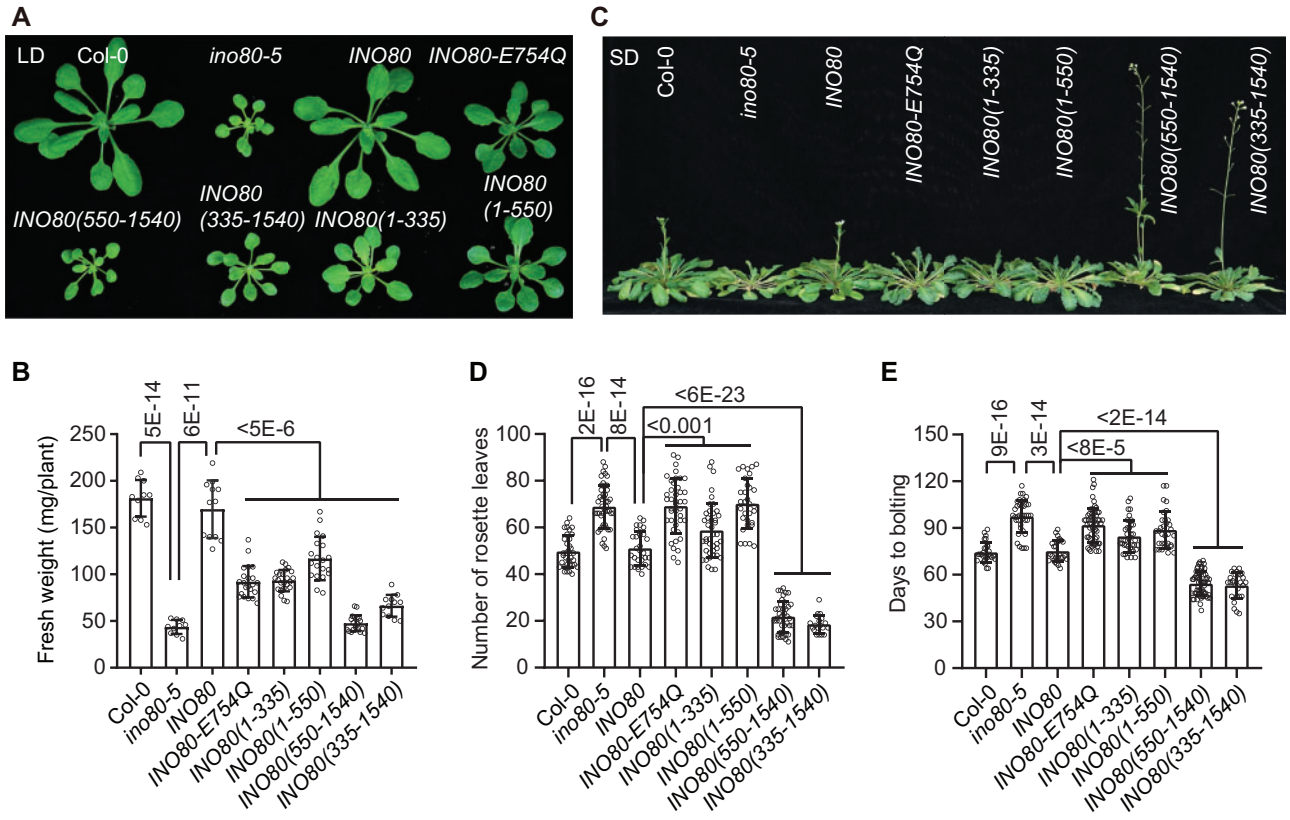

Figure 6 The INO80 NTD regulates vegetative growth and flowering time in an ATPase-independent manner. A, Morphological phenotypes of 22-day-old plants grown under LD conditions. Plants include Col-0, *ino80-5*, and the *ino80-5* mutant expressing full-length (INO80), mutated (INO80-E754Q), and truncated versions of INO80. The truncated INO80 versions are INO80(1–335 aa), INO80(1–550 aa), INO80(550–1540 aa), and INO80(335–1540 aa). B, Fresh weight of 22-day-old plants grown under LD conditions. Values are means ± SD from at least 10 plants for each genotype. C, Flowering time of Col-0, *ino80-5*, and the *ino80-5* mutant expressing full-length, mutated, and truncated versions of INO80 grown under SD conditions. D and E, Number of rosette leaves (D) and day to bolting (E) of plants grown under SD conditions. Values are means ± SD from at least 19 plants. *P*-values were determined by Student's *t*-test.

truncated transgenes encoding INO80 (1–335 aa) and INO80 (1–550 aa), was restored to a lesser extent by the truncated transgene encoding INO80 (335–1540 aa), but was only slightly restored by the truncated transgene encoding INO80 (550–1540 aa) (Figure 6, A and B; Supplemental Figure S15). These results suggest that the NTD can function independently of the ATPase domain to promote vegetative growth. We also generated transgenic plants that express the full-length INO80 harboring an E754Q mutation in the conserved ATPase domain, which disrupts the catalytic activity of the ATPase domain (Chen et al., 2011; Supplemental Figures S11 and S12). We found that the growth retardation of the *ino80-5* mutant can be partially complemented by the mutated *INO80* transgene (Figure 6, A and B; Supplemental Figure S15), suggesting that INO80 has an ATPase-independent function in regulating plant growth. Given that the growth retardation of *ino80-5* can be restored by the truncated INO80 (1–335 aa) as well as by the full-length INO80 harboring the E754Q mutation (Figure 6, A and B; Supplemental Figure S15), we propose that the INO80 NTD plays a major role in the ATPase-independent function of INO80.

We next investigated how the truncated *INO80* transgenes affect the flowering time of the *ino80-5* mutant under SD conditions. Although the *ino80-5* mutant showed a delayed flowering phenotype under SD conditions, the full-length *INO80* completely complemented the late-flowering phenotype of the *ino80-5* mutant (Figure 6, C–E). The flowering time of the *ino80-5* mutant plants expressing the truncated transgenes encoding INO80(1–335 aa) and INO80(1–550 aa) remained significantly delayed relative to the WT under SD conditions (Figure 6, C–E). Moreover, the flowering time of the *ino80-5* mutant plants that express the full-length INO80 construct harboring an E754Q mutation in the conserved ATPase domain was also significantly delayed relative to the WT (Figure 6, C–E). Therefore, the catalytic activity of the INO80 C-terminal ATPase domain is not only necessary for plant growth but is also necessary for promotion of flowering.

In contrast to the late-flowering phenotype of the *ino80-5* mutant plants expressing INO80(1–335 aa) or INO80(1–550 aa), the flowering time of the *ino80-5* mutant plants expressing INO80(335–1540 aa) and INO80(550–1540 aa) was markedly earlier than that of the WT under SD conditions

(Figure 6, C–E), suggesting that the INO80 NTD is responsible for delaying flowering time. Thus, the function of the NTD is opposite to that of the ATPase domain in regulating flowering time even though they cooperate to promote vegetative growth. Given that the INO80 accessory subunits assembled on the INO80 NTD are also responsible for suppression of flowering (Figure 2, C–E), we predicted that the INO80 NTD suppresses flowering by cooperating with the accessory subunits assembled on the NTD.

INO80 accessory subunits assembled on the INO80 NTD contributes to transcriptional activation by promoting H3K4 trimethylation

To investigate how the INO80 accessory components regulate gene expression, we performed RNA sequencing (RNA-seq) in the WT; in the *ino80-5*, *atx4/5 jmj24*, *nfrkb1/2/3*, *uch1/2*, and *arp5* mutants; and in the *ino80-5* mutant harboring the full-length *INO80* and the truncated *INO80* transgenes encoding INO80(1–550 aa) and INO80(335–1540 aa). The RNA-seq data identified a number of differentially expressed genes (DEGs) in each of the mutants relative to the WT (Figure 7, A and B; Supplemental Data set S2 and S3). In the *ino80-5* mutant, we identified 606 upregulated and 698 downregulated genes under LD conditions and 1,011 upregulated genes and 764 downregulated genes under SD conditions (Figure 7, A and B; Supplemental Data set S2 and S3). A number of *ino80-5*-affected genes were co-regulated in the *atx4/5 jmj24*, *nfrkb1/2/3*, *uch1/2*, and *arp5* mutants (Figure 7, C and D), supporting the notion that these components function together in the INO80 complex to regulate gene expression. We performed gene ontology (GO) analysis to characterize the biological processes of the overlapping DEGs in *ino80-5* and *atx4/5 jmj24*. The results showed that genes involved in multiple developmental processes and in response to chitin, blue light, and phytohormone stimuli are overrepresented in the overlapping DEGs under LD and SD conditions (Supplemental Figure S16). Thus, the ATX4/5-containing COMPASS may function together with INO80 to regulate genes involved in these biological processes.

Consistent with the similar growth and flowering-time phenotypes between the mutants of NTD-interacting accessory subunits (*atx4/5 jmj24*, *nfrkb1/2/3*, and *uch1/2*) and the *ino80-5* mutant expressing the NTD-deleted INO80(335–

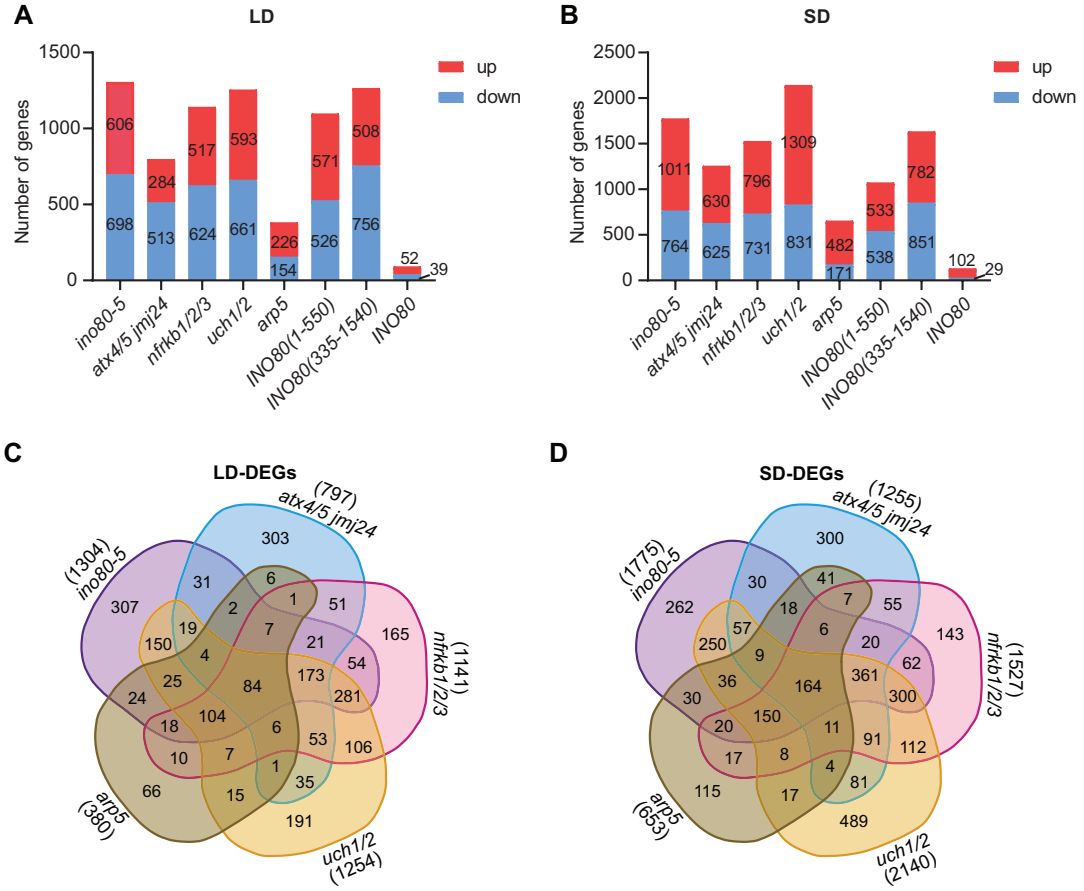

Figure 7 DEGs identified by RNA-seq analysis. A and B, Number of up and downregulated genes in indicated mutants relative to the WT under LD (A) and SD (B) conditions. C and D, Venn diagrams displaying unique and common DEGs identified in *ino80-5*, *atx4/5 jmj24*, *nfrkb1/2/3*, *uch1/2*, and *arp5* mutant plants relative to the WT under LD (C) and SD (D) conditions.

1540 aa), the gene expression change in the mutants of NTD-interacting accessory subunits and in the *ino80-5* mutant expressing the NTD-deleted INO80 was similar but was different from that in the mutant of ATPase domain-interacting accessory subunit (*arp5*) and in the *ino80-5* mutant expressing the ATPase domain-deleted INO80(1–550 aa) (Figure 8A). The effect of *nfrkb1/2/3* and *uch1/2* on the expression of *atx4/5 jmj24* downregulated genes was similar to that of the NTD-deleted INO80 but was significantly stronger than that of *arp5* and the ATPase domain-deleted INO80 under both LD and SD conditions (Figure 8B), confirming the ATPase-independent role of the INO80 NTD. These results support the notion that the INO80 accessory subunits that assemble on the INO80 NTD (COMPASS, NFRKB1/2/3, and UCH1/2) can regulate gene expression in an ATPase-independent manner.

Although the results shown above demonstrate that the INO80 NTD and the NTD-interacting accessory components are involved in an ATPase-independent function, it remains unknown how they regulate gene expression in an ATPase-independent manner. The conserved COMPASS is responsible for histone H3K4 trimethylation and thereby facilities transcriptional activation (Jiang et al., 2011; Smith et al., 2011; Fromm and Avramova, 2014; Chen et al., 2017). Considering that the ATX4/5-containing COMPASS interacts with the INO80 NTD, we determined whether INO80 promotes gene transcription by facilitating histone H3K4 trimethylation (H3K4me3). We, therefore, conducted H3K4me3 chromatin immunoprecipitation combined with sequencing (ChIP-seq) to determine whether the H3K4me3 level was affected in the *atx4/5 jmj24* and *ino80-5* mutants. We obtained 16,435 and 15,502 genes enriched with H3K4me3 in the Col-0 WT under LD and SD conditions, respectively, and most of these genes overlapped (88% for LD, 93% for SD) with H3K4me3-enriched genes as previously determined by ChIP-seq (Zhang et al., 2015b) (Supplemental Figure S17), suggesting that our H3K4me3 ChIP-seq data are reliable.

Based on the ChIP-seq data, we identified a number of genes with reduced H3K4me3 levels in the *atx4/5 jmj24* and *ino80-5* mutants relative to the WT under both LD and SD conditions (Supplemental Data set S4 and S5). By integrating RNA-seq and ChIP-seq data, we found that, while the H3K4me3 levels of the co-upregulated genes were not significantly affected in the *atx4/5 jmj24* and *ino80-5* mutants relative to the WT, the H3K4me3 levels of the co-downregulated genes were comparable in the *atx4/5 jmj24* and *ino80-5* mutants and were significantly lower than in the WT under both LD and SD conditions (Figures 7, C–D

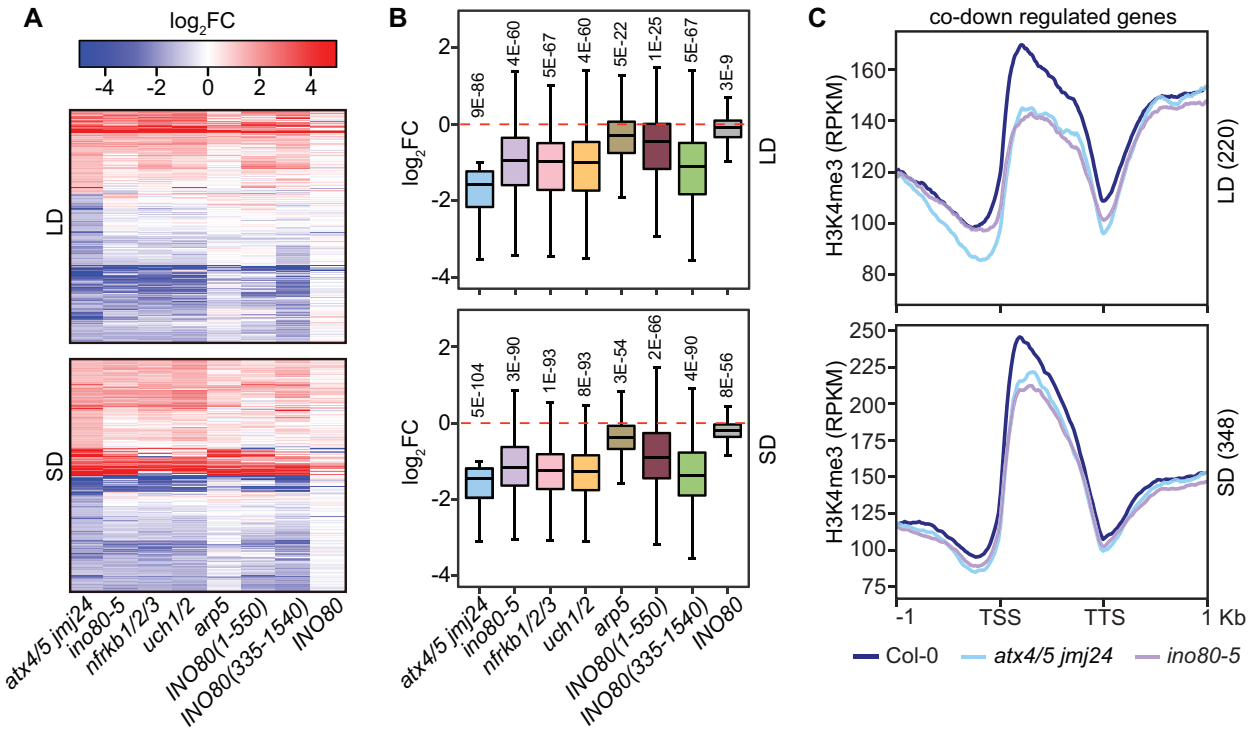

Figure 8 INO80 N-terminal-binding subunits co-regulate gene transcription. A, Heat maps showing expression patterns of DEGs ($\log_2(FC) > 1$ or $\log_2(FC) < -1$, $P < 0.01$) in *atx4/5 jmj24* compared with the WT under LD (upper) and SD (lower) conditions. B, Box-plots of RNA transcript levels in indicated samples based on downregulated genes ($\log_2(FC) < -1$, $P < 0.01$) in *atx4/5 jmj24* under LD (upper) and SD (lower) conditions. *P*-values were determined by Wilcoxon signed-rank test. C, Meta plots of H3K4me3 levels in Col-0, *atx4/5 jmj24*, and *ino80-5* at the 220 (LD, upper) or 348 (SD, lower) co-downregulated genes in *atx4/5 jmj24* and *ino80-5* from RNA-seq analysis data. TSS and TTS represent the transcription start site and the transcription termination site, respectively.

and 8C; Supplemental Figure S17). These results suggest that the ATX4/5-containing COMPASS module interacts with the NTD of INO80 in order to promote gene transcription by catalyzing H3K4me3 at a subset of INO80 target genes.

The H3K4me3-dependent role of the INO80 complex in transcriptional activation is independent of H2A.Z deposition

To investigate how gene expression is differentially regulated by the NTD and ATPase domains of INO80, we determined to what extent the DEGs identified in the *ino80-5* mutant are correlated with those identified in the *INO80(1–550 aa)* and *INO80(335–1540 aa)* complementation lines. The correlation analysis indicated that the expression of upregulated genes identified in *ino80-5* was positively correlated with that in *INO80(1–550 aa)* and *INO80(335–1540 aa)* complementation lines, but the expression of downregulated genes in *ino80-5* was more correlated with that in the *INO80(335–1540 aa)* complementation line (0.68 under LD and 0.67 under SD) than that in the *INO80(1–550 aa)* complementation line (0.49 under LD and 0.54 under SD) (Supplemental Figure S18), indicating that the NTD and ATPase domains are both related to the function of INO80 in transcriptional repression, whereas the NTD is more related to the function of INO80 in transcriptional activation.

Considering that H3K4me3 is associated with transcriptional activation, we investigated whether the transcriptional activation caused by the INO80-NTD is dependent on the histone H3K4 trimethyltransferase activity of ATX4/5. We defined overlapping DEGs identified in *ino80-5* and *INO80(1–550 aa)* but not in *INO80(335–1540 aa)* as genes regulated by the ATPase domain and the overlapping DEGs identified in *ino80-5* and *INO80(335–1540 aa)* but not in *INO80(1–550 aa)* as genes regulated by the NTD, and then determined the H3K4me3 levels of these genes (Figure 9, A and B). The results showed that the H3K4me3 levels were reduced at genes positively regulated by the NTD in both *atx4/5 jmj24* and *ino80-5* compared with the WT (Figure 9, A and B), suggesting that the ATX4/5-containing COMPASS is specifically involved in H3K4me3 at genes positively regulated by the NTD. The H3K4me3 levels of genes positively regulated by the ATPase domain were significantly reduced in *ino80-5* but not in *atx4/5 jmj24* compared with the WT (Figure 9, A and B). The reduced H3K4me3 levels of the ATPase domain-regulated genes identified in *ino80-5* are likely to be indirectly caused by reduced transcriptional levels of these genes. These analyses support the notion that the ATX4/5-containing COMPASS complex functions as an INO80-NTD-interacting module of the INO80 complex to promote gene transcription by mediating histone H3K4 trimethylation.

INO80 can contribute to H2A.Z deposition and transcriptional repression (Zhang et al., 2015a; Li et al., 2018; Yang et al., 2020). We then used recently published H2A.Z ChIP-seq data in WT and *ino80-5* (Yang et al., 2020) to determine whether H2A.Z deposition is differentially regulated at INO80-NTD and INO8O-ATPase regulated genes in the *ino80-5* mutant (Supplemental Figure S19). We found that increased levels of gene expression in the *ino80-5* mutant were correlated with reduced levels of H2A.Z at all INO80 target genes tested (Supplemental Figure S19), which is consistent with the previous report that the INO80 complex suppressed gene transcription by facilitating H2A.Z deposition (Zhang et al., 2015a; Yang et al., 2020). Unlike increased levels of gene expression that are correlated with reduced levels of H2A.Z in the *ino80-5* mutant, reduced levels of gene expression in the *ino80-5* mutant are either not correlated or only slightly correlated with the changes of H2A.Z levels (Supplemental Figure S19), suggesting that the H2A.Z is independent of the function of INO80 in transcriptional activation. These results further confirm that H3K4me3 mediated by the ATX4/5-containing COMPASS is important for the INO80 complex functioning in transcriptional activation.

To determine whether the INO80 complex mediates H3K4me3 and transcriptional activation by directly binding to its target chromatin loci, we performed ChIP followed by qPCR (ChIP-qPCR) for selected genes that are positively regulated by the INO80 NTD and by the NTD-interacting subunits. The results indicated that both the NTD-interacting subunits (ATX4, ATX5, JMJ24, and NFRKB1) and the ATPase domain-interacting subunit (ARP5) can associate not only with the genes that are co-regulated by the NTD and ATPase domains (*EMB2746* and *AT5G19500*) but also with the genes that are specifically regulated by the NTD (*BRS1* and *AT5G03130*) (Supplemental Figures S20 and S21), indicating that the INO80 complex components associate with its target genes as a whole even through the transcript levels of these genes were differentially regulated by the NTD-interacting module and the ATPase-interacting module.

Opposite effects of INO80 complex on the transcription of the flowering repressor genes *ARABIDOPSIS THALIANA HOMOBOX 1* and *FLC*

Among the genes with reduced H3K4me3 levels under SD conditions, a previously characterized flowering repressor gene, *ARABIDOPSIS THALIANA HOMOBOX 1* (*ATH1*; Proveniers et al., 2007), showed decreased H3K4me3 levels in *atx4/5 jmj24* as well as in *ino80-5* (Figure 9C; Supplemental Figure S22A). At the same time, the expression level of *ATH1* was significantly reduced in the *ino80-5* mutant and in the mutants of the INO80 NTD-interacting subunits, including *atx4/5 jmj24*, *nfrkb1/2/3*, and *uch1/2*, *yy1*, and was reduced to a lesser extent in the mutants of the HSA domain and ATPase domain-interacting subunits *arp9*, *arp5*, and *een-3* (Figure 9D; Supplemental Figure S22B). The reduction of the *ATH1* transcript level in *ino80-5* was almost completely restored by transgenes expressing the full-length INO80, the ATPase-mutated INO80 (INO80-E754Q), and the ATPase domain-deleted INO80 (INO80(1–335 aa) and INO80(1–550 aa)), but not by the transgene expressing the

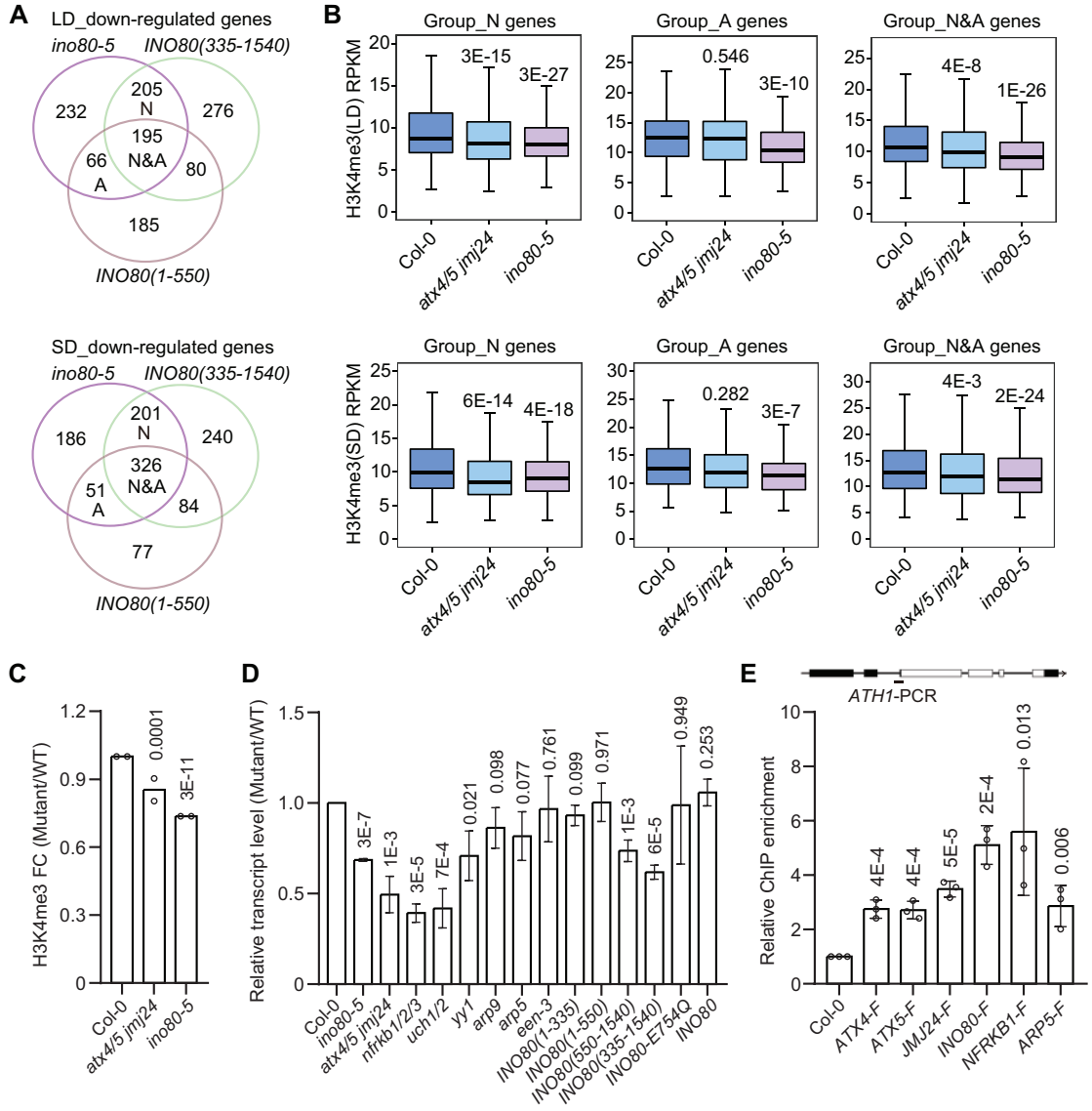

Figure 9 INO80 N-terminal-binding subunits stimulate gene transcription by promoting H3K4me3. A, Venn diagram showing the overlap of downregulated genes determined by RNA-seq analysis in the *ino80-5* mutant and in the *INO80(1–550 aa)* and *INO80(335–1540 aa)* complementation lines under LD (top) and SD (bottom) conditions. Group_N and Group_A genes are defined as genes positively regulated by the NTD and the ATPase domain of INO80, respectively. Group_N&A genes are defined as genes co-positively regulated by the NTD and ATPase domains of INO80. B, Box plots of H3K4me3 levels at Group_N, Group_A, and Group_N&A genes in Col-0, *atx4/5 jmj24*, and *ino80-5* under LD (top) and SD (bottom) conditions. *P*-values were calculated by Wilcoxon signed-rank test (for nonnormally distributed data) or Student's *t* test (for normally distributed data). C, Relative H3K4me3 levels of *ATH1* in WT, *atx4/5 jmj24*, and *ino80-5* mutant plants grown under SD conditions as determined by ChIP-seq. The FC (mutant/WT) of H3K4me3 levels at the peak region is shown. Values of FDR from ChIP-seq analysis are shown above the bars. D, Relative RNA transcript levels of *ATH1* in indicated plants grown under SD conditions as determined by RT-qPCR. Values are means ± SD from three biological replicates. *P*-values were determined by Student's *t* test. E, Determination of the association of ATX4, ATX5, JMJ24, INO80, NFRKB1, and ARP5 with the indicated region of *ATH1* by ChIP-qPCR in the *ATX4-Flag*, *ATX5-Flag*, *JMJ24-Flag*, *INO80-Flag*, *NFRKB1-Flag*, and *ARP5-Flag* transgenic plants and in the Col-0 negative control. Enrichment (y-axis) of Flag-tagged proteins was normalized to the input and the negative control *TA3*. Mean values from three independent biological replicates are shown with error bars. *P*-values were determined by Student's *t* test.

NTD-deleted INO80 (INO80(550–1540 aa) or INO80(335–1540 aa)) (Figure 9D; Supplemental Figure S22B). The associations of ATX4, ATX5, JMJ24, INO80, NFRKB1, and ARP5 with the *ATH1* gene were indicated by ChIP-qPCR (Figure 9E). These results suggest that the INO80 NTD and the NTD-interacting subunits but not the HSA and ATPase domains or their interacting subunits are responsible for facilitating the transcription of *ATH1* by promoting H3K4me3 in the INO80 complex.

Loss of *ATH1* has been shown to cause an early flowering phenotype under SD conditions (Proveniers et al., 2007). Thus, the reduced transcript levels of *ATH1* in the *atx4/5 jmj24*, *nfrkb1/2/3*, *uch1/2*, *yy1*, *INO80(335–1540 aa)*, and *INO80(550–1540 aa)* are consistent with the early flowering

phenotype of these plants under SD conditions, supporting the inference that the INO80 NTD and its interacting subunits are involved in promoting the expression of *ATH1* and thereby prevents early flowering under SD conditions. In the *ino80-5* mutant, however, the flowering time is delayed (Zhang et al., 2015a), even though the *ATH1* expression level is lower than in the WT (Figure 9D). Loss of *INO80* has been shown to cause reduction in H2A.Z deposition and elevation in transcription at the flowering repressor genes *FLC*, *MADS AFFECTING FLOWERING 4* (*MAF4*), and *MAF5* (Zhang et al., 2015a). Thus, the late-flowering phenotype of *ino80-5* can be at least partially explained by the increased expression of these flowering repressor genes. However, except for the *ino80-5* mutant, none of the INO80 accessory subunit mutants tested in this study exhibited late flowering, even though the expression levels of the flowering repressor genes *FLC* and *MAF5* are increased in these mutants (Supplemental Figure S23). Therefore, *ATH1* provides a possible explanation for the function of the INO80 NTD and the NTD-interacting subunits in regulating flowering time. Due to the complexity of the regulation of flowering time, further studies are required to investigate whether other flowering time regulators are involved in the regulation of flowering time by the INO80 complex.

Discussion

This study shows that the NTD of INO80 can interact with ATX4/5-containing COMPASS and the other subunits to form a functional NTD module and thereby mediate H3K4 trimethylation and transcriptional activation at a subset of INO80 target genes (Figure 10A). Although both NTD and ATPase domains are required for the normal growth of plants, the two domains show opposite effects on flowering. Different from the ATPase-dependent function of INO80 in promoting flowering, the NTD module of INO80 can suppress flowering under SD conditions. Deletion of the NTD module results in plant growth retardation and early flowering under SD conditions (Figure 10B). The recruitment of the ATX4/5-containing COMPASS into the INO80 complex may have specifically evolved in plants and provides an additional layer of complexity for the regulation of gene transcription involved in development and flowering.

Previous studies have indicated that the yeast and human INO80 complexes share nine conserved subunits: INO80, ARP4, ARP5, ARP8, IES2, IES6, YY1, RUVBL1, and RUVBL2 (Chen et al., 2013; Gerhold and Gasser, 2014). In addition, the human INO80 complex contains metazoan-specific subunits, including NFRKB, UCH37, MCRS1, INO80D, INO80E, and Amida. This study indicated that all of the subunits that are shared by yeast and humans are also shared by plants, suggesting that the INO80 complexes are conserved in eukaryotes. Moreover, as is the case in yeast and metazoans, all of the conserved accessory subunits are assembled on the INO80 ATPase domain in Arabidopsis, further supporting the inference that INO80 complexes are conserved among eukaryotes. We also found that the metazoan-specific accessory subunits NFRKB and UCH37 are present in the Arabidopsis INO80 complex, indicating that these subunits are not metazoan-specific but are shared by plants and metazoans. However, the metazoan-specific accessory subunits MCRS1, INO80D, INO80E, and Amida are not present in the Arabidopsis INO80 complex, suggesting that these subunits are definitely metazoan-specific. Moreover, we found plant-specific INO80 subunits, including the ATX4/5-containing COMPASS and the INO80-binding proteins INB1, INB2A, INB2B, and INB3. These analyses identified both conserved and plant-specific subunits of the INO80 complexes in Arabidopsis and demonstrated that the plant INO80 complexes show distinct characteristics from those in yeast and metazoans.

Our AP–MS identified five functionally redundant COMPASS complexes with each containing one of the five Trithorax-type histone H3K4 methyltransferases (ATX1-5).

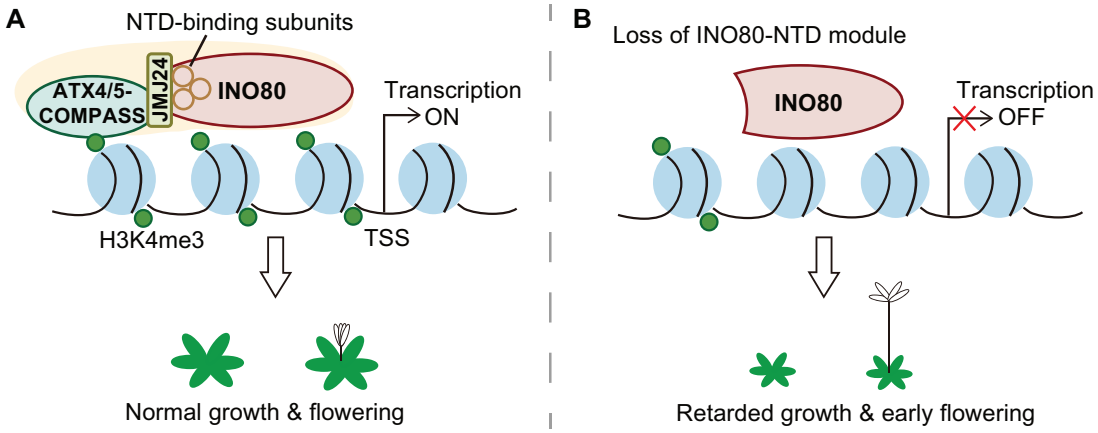

Figure 10 Model for the ATX4/5-containing COMPASS functioning as a module of Arabidopsis INO80 complex. A, The ATX4/5-containing COMPASS complex binds to the NTD of INO80 through JMJ24 to activate gene expression by catalyzing H3K4me3 at a subset of INO80 target genes. The ATX4/5-containing COMPASS complex and the other NTD-binding subunits of INO80 complex form NTD module that promotes plant growth and prevents precocious flowering under noninductive SD conditions. B, Loss of ATX4/5-containing COMPASS complex, the other NTD-binding subunits of INO80 complex, or the NTD of INO80 leads to retarded growth and early flowering of plants under SD conditions.

The complexes not only share the conserved subunits ATX1-5, WDR5A, TRO, and RBL but also contain unique subunits, such as JHDM2-type JmjC domain-containing histone demethylases JMJ24, JMJ26, and JMJ28. Based on composition of the five COMPASS complexes, they can be divided into three classes. The ATX1- and ATX2-containing complexes (Class I) and the ATX3-containing complex (Class II) share WDR5A, RBL, and TRO but contain different JMJ subunits. JMJ28 and JMJ26 are unique subunits of the Classes I and II COMPASS complexes, respectively. The ATX4- and ATX5-containing complexes (Class III) also share WDR5A, RBL, and TRO but contain another JMJ subunit, JMJ24. In humans, JMJD2B is an active histone H3K9 demethylase that can act as a subunit of the MLL2-containing COMPASS to coordinate H3K4 methylation and H3K9 demethylation (Shi et al., 2011). Unlike JMJD2B, which functions as an active histone demethylase in the human COMPASS complex, JMJ24 contains substitutions in the catalytic JmjC domain and cannot act as an active histone demethylase in Arabidopsis (Lu et al., 2008; Deng et al., 2015; Kabelitz et al., 2016). Although JMJ24 contains substitutions in the JmjC domain relative to the active JHDM2-type histone demethylase, the substitutions of the JmjC domain of JMJ24 remain conserved in plants (Kabelitz et al., 2016), suggesting that JMJ24 has been under positive selection during evolution and is functionally important even though it is not an active histone demethylase.

We found that JMJ24 acts as a bridge protein that is responsible for assembling the ATX4/5-containing COMPASS into the INO80 complex and showed that the interaction between ATX4/5-containing COMPASS and INO80 is required for maintaining the protein abundance of ATX4 and ATX5, supporting the inference that JMJ24 is functionally important. A previous genetic analysis showed that JMJ24 can counteract the active histone H3K9 demethylase IBM1 in the regulation of gene expression and development (Audonnet et al., 2017). The finding of JMJ24 in the COMPASS and INO80 complexes provides a plausible explanation for the involvement of JMJ24 in gene expression and development. JMJ24 was reported to have an ubiquitin E3 ligase activity and a histone H3 binding ability and to prevent transposon silencing (Deng et al., 2016; Kabelitz et al., 2016). The growth and flowering phenotypes of the *atx4/5 jmj24* triple mutant are more severe than those of the *atx4/5* double mutants and *jmj24* single mutants, which suggests that JMJ24 may have other activities in addition to acting as a bridge protein in the INO80 complex.

Our data show that, like in the INO80 complexes of yeast and metazoans, all of the identified INO80 accessory subunits are assembled on three INO80 domains in the Arabidopsis INO80 complex, that is, the NTD, HSA domain, and ATPase domain. As reported in yeast and metazoans, the ATPase and HSA domains and the accessory subunits assembled on them can interact with the nucleosome and function in catalyzing ATP hydrolysis and in remodeling nucleosomes (Chen et al., 2013; Gerhold and Gasser, 2014). However, how the NTD and the accessory subunits assembled on it are involved in the functioning of the INO80 complex remains to be investigated. By combining genetic and biochemical analyses, we demonstrated in this study that the INO80 NTD and the accessory subunits that assemble on it can function even without the INO80 ATPase domain. Our RNA-seq data showed that the ATPase-dependent and -independent functions are involved in regulating different sets of genes even though they cooperate to regulate a number of common genes, confirming that the INO80 complex has an ATPase-independent role. Considering that INO80 can act not only as a catalytic subunit for nucleosome remodeling but also as a scaffold for the assembly of accessory subunits, we predict that the accessory subunits assembled on the INO80 NTD may be responsible for the ATPase-independent function of INO80.

Among the accessory subunits assembled on the INO80 NTD, COMPASS is responsible for histone H3K4 trimethylation. The recruitment of COMPASS into the INO80 complex suggests that histone H3K4 trimethylation may at least partially contribute to the ATPase-independent activity of the INO80 complex. Consistent with the latter inference, our H3K4me3 ChIP-seq data indicate that INO80 is required for H3K4 trimethylation and transcriptional activation at INO80 NTD target genomic loci. Consistent with the previous studies (Zhang et al., 2015a; Yang et al., 2020), our analysis shows that the H2A.Z deposition catalyzed by INO80 is related to the function of INO80 in transcriptional repression. However, there is no obvious relationship between H2A.Z deposition and the transcription of genes activated by INO80, suggesting the function of the INO80 complex in transcriptional activation is independent of H2A.Z deposition mediated by the ATPase activity. In addition to COMPASS, NFRKB1/2/3, and UCH1/2 are also involved in the ATPase-independent function of INO80. In humans, the UCH1/2 ortholog UCH37 is a conserved deubiquitinating enzyme. In the INO80 complex, however, UCH37 is in an inactive state and can be activated by the interaction of the INO80 complex with the proteasome; NFRKB interacts with UCH37 and is responsible for inhibiting the deubiquitinating activity of UCH37 in the INO80 complex (Yao et al., 2008). Given that the assembly of the NFRKB and UCH orthologs on the INO80 NTD is conserved in plants and metazoans, the NTD of INO80 may be involved in regulating transcription by antagonizing the deubiquitinating activity in an ATPase-independent manner. YY1 is a conserved subunit of the INO80 complexes in plants and metazoans. The human YY1 exclusively interacts with the INO80 HSA domain and is necessary for the function of the INO80 complex in ATPase-dependent nucleosome remodeling (Chen et al., 2011). However, it remains to be investigated whether YY1 is involved in the ATPase-independent function of INO80. Our data indicate that the Arabidopsis YY1 interacts with both the NTD and HSA domain and participates in the ATPase-independent function of the INO80 complex even though the involvement of YY1 in the ATPase-dependent

role cannot be excluded. The human YY1 was reported to function as a transcriptional regulator in the INO80 complex (Cai et al., 2007). The involvement of YY1 in transcriptional regulation may represent another mechanism for the ATPase-independent function of the INO80 complex.

This study shows that the NTD module and ATPase domain of INO80 have antagonistic effects on flowering time. The antagonistic effects are probably important for the balance between vegetative growth and flowering under diverse environmental conditions. Under LD conditions, INO80 is responsible for promoting vegetative growth, thereby providing sufficient nutrients for reproduction. The accessory subunits that have been tested are involved in the promotion of vegetative growth but are dispensable for regulating flowering time under LD conditions. Considering that the effect of mutations on the vegetative growth is much weaker for the accessory subunits than for INO80, we predict that the vegetative growth in the mutants of the accessory subunits is sufficient for timely flowering. INO80 promotes vegetative growth and thereby facilitates flowering under both LD and SD conditions. However, SD conditions are not conducive for Arabidopsis flowering. It follows that under SD conditions, the positive effect of the INO80 ATPase domain on flowering must be antagonized. This study suggests that the accessory subunits assembled on the INO80 NTD have an ATPase-independent activity that can antagonize the function of the INO80 ATPase domain in promoting flowering while facilitating the function of INO80 in promoting vegetative growth, thus preventing precocious flowering under SD conditions.

In conclusion, this study not only demonstrates that the accessory subunits assembled on the NTD of INO80 have an ATPase-independent function but also reveals the possible mechanisms by which they regulate flowering time. Given that the composition and structure of INO80 complexes are highly conserved in eukaryotes (Bao and Shen, 2011; Chen et al., 2011; Kang et al., 2019), it will be interesting to determine whether the INO80 complexes in other eukaryotes also have an ATPase-independent function and how the ATPase-dependent and ATPase-independent functions are coordinated.

Materials and methods

Plant materials

All of the *A. thaliana* plants used in this study were in the Col-0 background. The *ino80-5* mutants (SALK_067880) were described previously (Zhang et al., 2015a). The T-DNA insertion lines were ordered from the Arabidopsis Biological Resource Center or the Nottingham Arabidopsis Stock Center, and included *atx4* (SALK_060156), *atx5* (CS831182), *jmj24* (SALK_021260), *nfrkb1* (SALK_125093), *nfrkb2* (SALK_008159), *nfrkb3* (SALK_125082), *inb3* (SALK_084761), *arp9* (SALK_076344), *arp5* (CS437022), and *yy1* (SALK_040806). The homozygous mutant lines were confirmed by PCR using primers listed in Supplemental Data set S6. The double mutants and triple mutants were generated by crossing the single mutant plants. The *inb1*, *inb2a/2b*, *uch1*, *uch2*, *uch1/2*, and *een-3* mutant plants were generated by the pHEE401E-CRISPR/Cas9 system (Wang et al., 2015). The transgene-free mutants were isolated and used in the experiments. Primers used for the construction of CRISPR/Cas9 vectors are listed in Supplemental Data set S6.

Full-length genomic regions of *ATX1*, *ATX2*, *ATX3*, *ATX4*, *ATX5*, *JMJ24*, *JMJ28*, *WDR5A*, *INO80*, *UCH1*, *UCH2*, *NFRKB1*, *NFRKB2*, *INB1*, *INB2A*, *INB2B*, *INB3*, *YY1*, *ARP9*, *IES2A*, *IES2B*, *ARP5*, and *EEN*, and the genomic sequence encoding truncated INO80 proteins, including INO80-(1–335 aa), INO80-(1–550 aa), INO80-(550–1540 aa), and INO80-(335–1540 aa), driven by their native promoters were cloned into lab-modified pCAMBIA1305-Flag or pCAMBIA1305-Myc vectors to construct the transgenic plants used for co-IP, AP–MS, and ChIP experiments. The AP–MS data of *RIN1-Flag* and *RIN2-Flag* transgenic plants were generated in our previous study (Luo et al., 2020). Plants carrying the *INO80-E754Q* or *JMJ24-H665A* single mutations were generated by using the PCR-based Mut Express II Fast mutagenesis Kit V2 (Vazyme, Nanjing, China; C215). Primers used for the construction of pCAMBIA1305 plasmids are listed in Supplemental Data set S6. To obtain plant materials used for co-IP, the *ATX4-Flag* and *ATX5-Flag* transgenic plants were crossed with *Myc*-tagged *INO80* or *JMJ24* transgenic plants to produce plants carrying both *Flag-* and *Myc*-tagged transgenes. *ATX4-Flag* and *ATX5-Flag* transgenic plants were crossed with the *jmj24* and *ino80-5* mutant plants, and the *pATX4:ATX4-Flag* and *pATX5:ATX5-Flag* transgenic plants in the WT background and in the *jmj24* and *ino80-5* mutant backgrounds were isolated in the F2 segregation groups.

Plant growth conditions

Seeds were surface-sterilized and sown on Murashige and Skoog (MS) medium plates or on MS medium plates containing hygromycin (30 mg/L) and ampicillin (50 mg/L) for screening transgenic plants. After they were sown on MS medium plates, the seeds were pretreated by exposure to 4°C for 2 days and were then transferred to a growth chamber with an LD photoperiod (23°C, 16-h light/22°C, 8-h darkness) or an SD photoperiod (23°C, 8 h light/22°C, 16 h darkness). Light is provided by white light fluorescent tubes (Philips, Amsterdam, Netherlands; F17T8/TL841) at 100 μmol/m^2/s. After 10 days, the seedlings were transferred to soil and were grown under greenhouse conditions with the same diurnal cycle of photoperiod and temperature.

Determination of plant flowering time and growth

Arabidopsis flowering time was described in terms of number of days until bolting and rosette leaf number. The days to bolting were scored beginning with the appearance of a 1-cm-long florescence, and the numbers of rosette leaves were then counted. When plants were 22 days old, their aboveground fresh weight and rosette diameter were determined.

Phylogenetic analysis and sequence alignments

Sequences of INB1, INB2A, INB2B, and INB3 homologs were retrieved by a BLASTP search against the NCBI protein database and TAIR database. Multiple alignments of the amino acid sequences were created with the ClustalW algorithm (Thompson et al., 1994). A phylogenetic tree was constructed and visualized by MEGA X software using a maximum likelihood analysis and Jones, Taylor, and Thorton matrix-based model. Bootstrapping was performed with 1,000 replications (Kumar et al., 2018). Alignment files are provided as Supplemental File S1.

RT-qPCR, RNA deep sequencing, and data analysis

Total RNA was extracted with TRIzol reagent (Invitrogen, Waltham, MA, USA; 15596018) from seedlings grown on MS plates. The seedlings were grown for 11 days under LD conditions (16-h light, 8-h darkness) and for 14 days under SD conditions (8-h light, 16-h darkness).

For RT-qPCR, 2 μg RNA was used for DNase digestion and reverse transcription using 5×All-In-One RT MasterMix (ABM, New York, NY, USA; G492). The transcribed cDNA underwent qPCR using KAPA SYBR FAST qPCR Master Mix (KAPA, Wilmington, MA, USA; KK4601). The reference gene *ACT2* was used for normalization of qPCR-derived gene expression. Primers used for RT-qPCR are listed in Supplemental Data set S6. For RNA deep sequencing-based transcriptome analysis, two independent biological RNA replicates were sent to BGI (Shenzhen, China) for the construction of sequencing libraries and deep sequencing with an DNBSEQ platform (single-end 50-bp reads). After removal of adapters and low-quality reads, the clean reads were aligned to the Arabidopsis genome (TAIR10) using HISAT2 version 2.2.0 with the default parameters (Kim et al., 2019). DEGs were identified with $|\log2FC| > 1$ and $P < 0.01$ using edgeR (Robinson et al., 2010). GO analysis was performed using the clusterProfiler in the R package (Yu et al., 2012). The heatmap was drawn by R package gplots based on the log2FC values (Warnes et al., 2020). The box plots were drawn using the geom_boxplot function of the R library ggplot2 using log2FC values (Wickham, 2016).

Y2H assay

The entire coding regions and several truncated derivatives of *ATX4*, *ATX5*, and *JMJ24* were cloned into the plasmids pGBKT7 (BD) and pGADT7 (AD). Primers used for the cloning are listed in Supplemental Data set S6. The AD and BD plasmids were co-transformed into yeast strain AH109 and were spread on the synthetic dropout medium without tryptophan and leucine (SD-WL). Colonies growing on the SD-WL medium were suspended in distilled H_2O and then spotted on SD medium without tryptophan, leucine, and histidine (SD-WLH) and on SD-WLH medium supplemented with 3-amino-1,2,4-triazole.

Co-IP and AP–MS

Co-IP and AP–MS were performed to detect protein–protein interactions. For co-IP, 1 g of male/female parents and F1 generation seedlings was ground into powder in liquid nitrogen. For AP–MS, 3 g of seedlings or inflorescence tissues was ground. The samples were resuspended in 5 mL (for co-IP) or 15 mL (for AP–MS) of ice-cold lysis buffer (50 mM Tris–HCl, pH 7.6, 150 mM NaCl, 5 mM $MgCl_2$, 10% glycerol, 0.1% NP-40, 0.5 mM DTT, 1 mM PMSF, one tablet of Roche protease inhibitor cocktail per 50 mL) and incubated for 20 min at 4°C, followed by centrifugation at 12,000 *g* for 15 min. The supernatant was passed through two layers of Miracloth into a 15-mL centrifuge tube, and the filtrate was incubated with 30 μL (for co-IP) or 100 μL (for AP–MS) of anti-Flag M1 Agarose affinity gel (Sigma, St Louis, MO, USA; A4596) for 2.5 h at 4°C. The agarose beads were collected by gentle centrifugation and were washed in lysis buffer 5 times to remove nonspecific binding proteins. Proteins specifically binding to the beads were eluted with 100 μL of lysis buffer containing 15 μg of 3×Flag peptides (Sigma, F4799). For co-IP analysis, the input samples and elution fractions were subjected to immunoblot analysis with anti-Flag (Sigma, F1804) and anti-Myc (Abmart, Shanghai, China; M20002) antibodies. For AP–MS, elution profiles were run on a 10% SDS–PAGE gel, which was followed by silver staining with ProteoSilver Silver Stain Kit (Sigma, PROT-SIL1). Subsequent mass spectrometry analysis of the silver-stained proteins was performed as previously described (Tan et al., 2020). In brief, the silver-stained gels were excised and de-stained before in-gel digestion with trypsin overnight at 37°C. Following enzymatic digestion, the peptides were eluted on a capillary column and sprayed into a Q Exactive Mass Spectrometer equipped with a nano-ESI ion source (Thermo Fisher Scientific, Waltham, MA, USA). The acquired spectra were searched in the International Protein Index database of Arabidopsis on the Mascot server (Matrix Science, London, UK).

The WT Col-0 was used as a negative control of AP–MS. Proteins detected both in the Col-0 and transgenic plants were removed from the candidate interacting proteins list. However, due to the nonspecific binding of the anti-Flag M1 Agarose affinity gel, small numbers of queries matched with INO80, RIN1, RIN2, ARP4/5/9, YY1, UCH1, NFRKB2, and JMJ24 could also be detected in the Col-0 background sometimes. In order to remove the background noise of these proteins, we calculated the average value of matched queries data of five independent AP–MS results of Col-0 (Supplemental Data set S1) for the above proteins and then took this average value from the matched queries of the corresponding protein identified in *Flag*-tagged transgenic plants.

For AP–MS data analysis, the matched queries were normalized to the protein amino acid residues length and total queries of the protein complex to get Normalized Spectral Abundance Factors (NSAFs) as previously described with minor modifications (Florens et al., 2006):

$$\mathrm{NSAF} = 100 \times \frac{\mathrm{Spectra}/\mathrm{Length}}{\sum_{i=1}^{N} (\mathrm{Spectra}/\mathrm{Length})_i}$$

The normalized AP–MS data were visualized by heatmap.2 in gplots R package. The protein complex network was drawn from AP–MS data using Cytoscape software.

Protein purification and pull-down assay

The cDNA sequence encoding N-terminal region of INO80(1–550 aa) was cloned into the *pGEX6P-1* vector and then transformed into *Escherichia coli* strain (DE3). The cell culture was incubated at 37°C until the OD_{600} reached 0.8. IPTG was added to a final concentration of 0.1 mM for induction of protein expression at 16°C for 16 h. Cells were collected by centrifugation and lysed by GST-lysis buffer (20 mM Tris–HCl, pH 7.6, 150 mM NaCl, 1 mM PMSF, 1 mM DTT) followed by sonication and centrifugation at 38,000 *g* for 1 h. The supernatant was filtered and then incubated with GST beads (GE Healthcare, Chicago, IL, USA; 17-0756-01) for 2 h at 4°C. After washing by GST-lysis buffer, the GST-fusion protein was eluted by fresh GSH elution buffer (50 mM Tris–HCl, pH 8.0, 150 mM NaCl, 20 mM Glutathione, 1 mM DTT). The *JMJ24* cDNA sequence appended the C-terminal His tag was cloned into pAT423 (Ishii et al., 2014). The JMJ24-His fusion protein was expressed in yeast strain YPH499. The yeast cells were ground in liquid nitrogen and lysed with buffer containing 50 mM Tris–HCl, pH 7.5, 1 mM EDTA (AMRESCO, USA; 0105-1KG), pH 8.0, 150 mM NaCl, 0.05% NP-40, 20 mM imidazole, 10% glycerol, 1 mM PMSF, 1 mM DTT, and one tablet of Roche protease inhibitor cocktail per 50 mL. JMJ24-His was purified from the yeast extract using Ni-NTA His Bind Resin (Millipore, Burlington, MA, USA; 70666-5).

For the GST pull-down assay, GST-INO80(1–550 aa) or GST proteins were incubated with JMJ24-His and GST beads in 1 mL GST lysis buffer for 1 h at 4°C. After washing 6 times with lysis buffer, the proteins were eluted with GSH elution buffer. About 10% input and elution samples were analyzed by immunoblotting using anti-GST antibody (Abmart; M20007S) and anti-His antibody (ORIGENE, Rockville, MD, USA; TA150088).

ChIP assay and data analysis

The ChIP-seq assay was performed as previously described (Zhao et al., 2019). A 2-g quantity of seedlings was ground into a fine powder in liquid nitrogen and crosslinked in 15 mL of ice-cold NEB buffer (20 mM Tris–HCl, pH 7.5, 20 mM KCl, 2 mM EDTA, pH 8.0, 2.5 mM $MgCl_2$, 25% glycerol, 250 mM sucrose, 5 mM DTT, 1 mM PMSF, and one tablet of Roche protease inhibitor cocktail per 50 mL) with 1% formaldehyde for 20 min at 4°C with gentle shaking. The solution was passed through two layers of Miracloth. Nuclei were collected by centrifugation and were washed 4 or 5 times with NRBT buffer (20 mM Tris–HCl, pH 7.5, 2.5 mM $MgCl_2$, 25% glycerol, and 0.2% Triton X-100). Nuclei were lysed with NLS buffer (20 mM Tris–HCl, pH 8.0, 2 mM EDTA, pH 8.0, 0.2% NP-40, 1 mM PMSF, and one tablet of Roche protease inhibitor cocktail per 50 mL). The chromatin was fragmented by sonication at 4°C and was diluted with Dilution Buffer (20 mM Tris–HCl, pH 8.0, 2 mM EDTA, pH 8.0, 200 mM NaCl, 1 mM PMSF, and protease inhibitor cocktail). For H3K4me3-ChIP analysis, the chromatin was precleared by incubation with 40 μL of protein A magnetic beads (Thermo Fisher, 10001D) for 2 h. After removal of the beads, the chromatin was incubated with 3 μL of anti-H3K4me3 antibody (Millipore; 07-473) overnight. The next day, 40 μL of Protein A beads was added to the chromatin sample, which was then incubated for 2–4 h. For Flag-ChIP, 100 μL Anti-FLAG M2 Magnetic Beads (Sigma, M8823) were incubated with the chromatin overnight. After five washes with Binding/Washing buffer (20 mM Tris–HCl, pH 8.0, 2 mM EDTA, 150 mM NaCl, 0.1% Triton X-100, and 1 mM PMSF) and two washes with TE buffer (10 mM Tris–HCl, pH 8.0, and 1 mM EDTA), crosslinked protein–DNA complexes were eluted with Elution Buffer (100 mM $NaHCO_3$ and 1% SDS). The eluate was subsequently subjected to reverse crosslinks, RNase digestion, and Proteinase K digestion. DNA was purified by phenol/chloroform/isoamyl alcohol extraction and was precipitated with isopropanol.

For H3K4me3-ChIP seq analysis, the ChIP-seq libraries were generated using the NEBNext® Ultra™ DNA Library Prep Kit for Illumina®(NEB, Ipswich, MA, USA) by the Novogene Corporation (Beijing, China). For data analysis, after adapter and low-quality reads were removed, the clean reads were aligned to the Arabidopsis genome (TAIR10) using Bowtie2 allowing one mismatch (Langmead and Salzberg, 2012). Enriched H3K4me3 regions were identified by MACS2 with default parameters (Zhang et al., 2008). Spatial-clustering method for identification of ChIP-enriched regions (SICER) was used to identify differentially enriched peaks between the WT and each of the mutants with false discovery rate (FDR) < 0.05, fold change (FC) of reads in the mutant as compared with the WT (mutant/WT) <0.9 or FC (mutant/WT) >1.1 (Zang et al., 2009). The signal profiles were drawn by deepTools (Ramirez et al., 2016). For Flag-ChIP qPCR, 0.5 μL of ChIP DNA was used as templates. Enrichments of ATX4, ATX5, JMJ24, INO80, NFRKB1, and ARP5 on target genes were normalized to that on the *TA3* locus. Primers used for ChIP-qPCR were listed in Supplemental Data set S6.

Data availability statement

Raw RNA-seq and ChIP-seq data have been deposited in the Gene Expression Omnibus database with the accession code GSE162375.

Accession numbers

Accession numbers of genes reported in this study include: AT2G31650 (*ATX1*), AT1G05830 (*ATX2*), AT3G61740 (*ATX3*), AT4G27910 (*ATX4*), AT5G53430 (*ATX5*), AT1G09060 (*JMJ24*), AT1G11950 (*JMJ26*), AT4G21430 (*JMJ28*), AT3G49660 (*WDR5A*), AT1G51450 (*TRO*), AT3G21060 (*RBL*), AT3G57300 (*INO80*), AT5G16310 (*UCH1*), AT1G65650 (*UCH2*), AT3G45830 (*NFRKB1*), AT5G13950 (*NFRKB2*), AT1G02290 (*NFRKB3*), AT4G18400 (*INB1*), AT4G30630 (*INB2A*), AT5G57910 (*INB2B*), AT3G51500 (*INB3*), AT4G06634 (*YY1*), AT1G18450 (*ARP4*), AT5G43500 (*ARP9*), AT2G47350 (*IES2A*), AT3G06660 (*IES2B*), AT1G56460 (*IES2C*), AT5G22330 (*RIN1*), AT5G67630 (*RIN2*), AT3G12380 (*ARP5*), AT4G38495 (*EEN*), and AT4G32980 (*ATH1*).

Supplemental data

The following materials are available in the online version of this article.

Supplemental Figure S1. Phylogenetic analyses of orthologs of INB1, INB2A/2B, and INB3 in different plant species.

Supplemental Figure S2. Detection of the interactions of ATX4 or ATX5 with JMJ24 by co-IP.

Supplemental Figure S3. Mutations in *UCH1*, *UCH2*, *EEN*, *INB1*, *INB2A*, and *INB2B* generated by the CRISPR/Cas9 system.

Supplemental Figure S4. Rosette diameter of WT and INO80 complex mutant plants.

Supplemental Figure S5. Retarded growth phenotypes of the *nfrkb1/2* mutant were restored by *NFRKB1-Flag* and *NFRKB2-Flag* transgenes.

Supplemental Figure S6. Retarded growth phenotypes of *uch1/2* mutants were restored by *UCH1-Flag* or *UCH2-Flag* transgenes.

Supplemental Figure S7. Retarded growth phenotypes of *atx4/5* mutants were restored by *ATX4-Flag* or *ATX5-Flag* transgenes.

Supplemental Figure S8. The retarded growth phenotypes of *jmj24* mutants were restored by *JMJ24-Flag* transgenes.

Supplemental Figure S9. Phenotypic analyses of WT, *inb1*, *inb2a/2b*, and *inb3* mutants.

Supplemental Figure S10. The flowering time of *atx4/5*, *jmj24*, *atx4/5 jmj24*, *nfrkb1/2/3*, and *uch1/2* mutant plants did not significantly differ from that of the WT under LD conditions.

Supplemental Figure S11. Multiple sequence alignment of INO80 orthologs in human, yeast, and Arabidopsis.

Supplemental Figure S12. Expression of WT and mutated full-length *INO80* transgenes and truncated *INO80* transgenes as determined by immunoblotting.

Supplemental Figure S13. Interactions between JMJ24 and ATX4/5 as determined by Y2H assays.

Supplemental Figure S14. The protein levels of JMJ24 and INO80 are unaffected in the *atx4/5* double mutant.

Supplemental Figure S15. Rosette diameters of the WT, *ino80-5*, and *ino80-5* mutant plants carrying full-length, mutated, and truncated *INO80* transgenes.

Supplemental Figure S16. GO analysis of the overlapping DEGs identified in *atx4/5 jmj24* and *ino80-5* mutants under LD and SD conditions.

Supplemental Figure S17. H3K4me3 enriched genes in Col-0 and H3K4me3 enrichment at co-upregulated genes in *atx4/5 jmj24* and *ino80-5*.

Supplemental Figure S18. Scatter plots showing the correlation of the expression changes of up and downregulated genes in *ino80-5* between *ino80-5* and *INO80(1–550 aa)* or *INO80(335–1540 aa)* transgenic plants.

Supplemental Figure S19. H2A.Z levels at genes regulated by NTD and ATPase domain of INO80 in WT and *ino80-5* mutants.

Supplemental Figure S20. Determination of the protein levels of INO80, JMJ24, ATX4, ATX5, NFRKB1, and ARP5 in the plant materials used for ChIP experiments.

Supplemental Figure S21. ATX4/5-containing COMPASS functions in the INO80 complex to promote gene transcription.

Supplemental Figure S22. The relative H3K4me3 and transcript levels at *ATH1* as determined by H3K4me3 ChIP-seq and RNA-seq.

Supplemental Figure S23. The relative transcript levels of *MAF5* and *FLC* as determined by RNA-seq analysis.

Supplemental Data set S1. Full list of proteins identified by AP–MS.

Supplemental Data set S2. DEGs under LD conditions.

Supplemental Data set S3. DEGs under SD conditions.

Supplemental Data set S4. List of genes with reduced H3K4me3 levels in *atx4/5 jmj24* and *ino80-5* under LD conditions.

Supplemental Data set S5. List of genes with reduced H3K4me3 levels in *atx4/5 jmj24* and *ino80-5* under SD conditions.

Supplemental Data set S6. Primers were used in this study.

Supplemental File S1. Sequence alignments of INB1, INB2A/2B, and INB3 orthologs in different plant species.

Funding

This work was supported by the National Natural Science Foundation of China (32025003) and by the National Key Research and Development Program of China (2016YFA0500801) from the Chinese Ministry of Science and Technology.

Conflict of interest statement. The authors declare no conflict of interest.

References

Alvarez-Venegas R, Avramova Z (2012) Evolution of the PWWP-domain encoding genes in the plant and animal lineages. BMC Evol Biol **12**: 101

Aramayo RJ, Willhoft O, Ayala R, Bythell-Douglas R, Wigley DB, Zhang X (2018) Cryo-EM structures of the human INO80 chromatin-remodeling complex. Nat Struct Mol Biol **25**: 37–44

Aslam M, Fakher B, Jakada BH, Cao S, Qin Y (2019) SWR1 chromatin remodeling complex: a key transcriptional regulator in plants. Cells **8**: 1621

Audonnet L, Shen Y, Zhou DX (2017) JMJ24 antagonizes histone H3K9 demethylase IBM1/JMJ25 function and interacts with RNAi pathways for gene silencing. Gene Exp Patterns **25**: 1–7

Ayala R, Willhoft O, Aramayo RJ, Wilkinson M, McCormack EA, Ocloo L, Wigley DB, Zhang X (2018) Structure and regulation of the human INO80–nucleosome complex. Nature **556**: 391–395

Bao Y, Shen X (2011) SnapShot: chromatin remodeling: INO80 and SWR1. Cell **144**: 158–158 e152

Cai Y, Jin J, Yao T, Gottschalk AJ, Swanson SK, Wu S, Shi Y, Washburn MP, Florens L, Conaway RC (2007) YY1 functions with INO80 to activate transcription. Nat Struct Mol Biol **14**: 872–874

Chen LQ, Luo JH, Cui ZH, Xue M, Wang L, Zhang XY, Pawlowski WP, He Y (2017) ATX3, ATX4, and ATX5 encode putative H3K4

methyltransferases and are critical for plant development. Plant Physiol **174**: 1795–1806

Chen L, Conaway RC, Conaway JW (2013) Multiple modes of regulation of the human Ino80 SNF2 ATPase by subunits of the INO80 chromatin-remodeling complex. Proc Natl Acad Sci USA **110**: 20497–20502

Chen L, Cai Y, Jin J, Florens L, Swanson SK, Washburn MP, Conaway JW, Conaway RC (2011) Subunit organization of the human INO80 chromatin remodeling complex an evolutionarily conserved core complex catalyzes ATP-dependent nucleosome remodeling. J Biol Chem **286**: 11283–11289

Clapier CR, Cairns BR (2009) The biology of chromatin remodeling complexes. Annu Rev Biochem **78**: 273–304

Deng S, Jang IC, Su L, Xu J, Chua NH (2016) JMJ24 targets CHROMOMETHYLASE3 for proteasomal degradation in Arabidopsis. Genes Dev **30**: 251–256

Deng S, Xu J, Liu J, Kim SH, Shi S, Chua NH (2015) JMJ24 binds to RDR2 and is required for the basal level transcription of silenced loci in Arabidopsis. Plant J **83**: 770–782

Ding Y, Avramova Z, Fromm M (2011) The Arabidopsis trithorax-like factor ATX1 functions in dehydration stress responses via ABA-dependent and ABA-independent pathways. Plant J **66**: 735–744

Eustermann S, Schall K, Kostrewa D, Lakomek K, Strauss M, Moldt M, Hopfner KP (2018) Structural basis for ATP-dependent chromatin remodelling by the INO80 complex. Nature **556**: 386–390

Flaus A, Martin DM, Barton GJ, Owen-Hughes T (2006) Identification of multiple distinct Snf2 subfamilies with conserved structural motifs. Nucleic Acids Res **34**: 2887–2905

Florens L, Carozza MJ, Swanson SK, Fournier M, Coleman MK, Workman JL, Washburn MP (2006) Analyzing chromatin remodeling complexes using shotgun proteomics and normalized spectral abundance factors. Methods **40**: 303–311

Fritsch O, Benvenuto G, Bowler C, Molinier J, Hohn B (2004) The INO80 protein controls homologous recombination in *Arabidopsis thaliana*. Mol Cell **16**: 479–485

Fromm M, Avramova Z (2014) ATX1/AtCOMPASS and the H3K4me3 marks: how do they activate Arabidopsis genes? Curr Opin Plant Biol **21**: 75–82

Gerhold CB, Gasser SM (2014) INO80 and SWR complexes: relating structure to function in chromatin remodeling. Trends Cell Biol **24**: 619–631

Gu BW, Tan LM, Zhang CJ, Hou XM, Cai XW, Chen S, He XJ (2020) FHA2 is a plant-specific ISWI subunit responsible for stamen development and plant fertility. J Integr Plant Biol **62**: 1703–1716

Han SK, Wu MF, Cui S, Wagner D (2015) Roles and activities of chromatin remodeling ATP ases in plants. Plant J **83**: 62–77

Hyun K, Jeon J, Park K, Kim J (2017) Writing, erasing and reading histone lysine methylations. Exp Mol Med **49**: e324

Inagaki S, Miura-Kamio A, Nakamura Y, Lu F, Cui X, Cao X, Kimura H, Saze H, Kakutani T (2010) Autocatalytic differentiation of epigenetic modifications within the Arabidopsis genome. EMBO J **29**: 3496–3506

Ishii J, Kondo T, Makino H, Ogura A, Matsuda F, Kondo A (2014) Three gene expression vector sets for concurrently expressing multiple genes in Saccharomyces cerevisiae. FEMS Yeast Res **14**: 399–411

Jha S, Dutta A (2009) RVB1/RVB2: running rings around molecular biology. Mol Cell **34**: 521–533

Jiang D, Kong NC, Gu X, Li Z, He Y (2011) Arabidopsis COMPASS-like complexes mediate histone H3 lysine-4 trimethylation to control floral transition and plant development. PLoS Genet **7**: e1001330

Kabelitz T, Brzezinka K, Friedrich T, Górka M, Graf A, Kappel C, Bäurle I (2016) A jumonji protein with E3 ligase and histone H3 binding activities affects transposon silencing in Arabidopsis. Plant Physiol **171**: 344–358

Kandasamy MK, McKinney EC, Deal RB, Smith AP, Meagher RB (2009) Arabidopsis actin-related protein ARP5 in multicellular development and DNA repair. Dev Biol **335**: 22–32

Kang H, Zhang C, An Z, Shen WH, Zhu Y (2019) AtINO80 and AtARP5 physically interact and play common as well as distinct roles in regulating plant growth and development. New Phytol **223**: 336–353

Kapoor P, Shen X (2014) Mechanisms of nuclear actin in chromatin-remodeling complexes. Trends Cell Biol **24**: 238–246

Kim D, Paggi JM, Park C, Bennett C, Salzberg SL (2019) Graph-based genome alignment and genotyping with HISAT2 and HISAT-genotype. Nat Biotechnol **37**: 907–915

Klose RJ, Kallin EM, ZhangY (2006) JmjC-domain-containing proteins and histone demethylation. Nat Rev Genet **7**: 715–727

Kumar S, Stecher G, Li M, Knyaz C, Tamura K (2018) MEGA X: molecular evolutionary genetics analysis across computing platforms. Mol Biol Evol **35**: 1547–1549

Langmead B, Salzberg SL (2012) Fast gapped-read alignment with Bowtie 2. Nat Methods **9**: 357–359

Li C, Liu Y, Shen WH, Yu Y, Dong A (2018) Chromatin-remodeling factor OsINO80 is involved in regulation of gibberellin biosynthesis and is crucial for rice plant growth and development. J. Integr Plant Biol **60**: 144–159

Li D, Liu J, Liu W, Li G, Yang Z, Qin P, Xu L (2017) The ISWI remodeler in plants: protein complexes, biochemical functions, and developmental roles. Chromosoma **126**: 365–373

Liu Y, Zhang A, Yin H, Meng Q, Yu X, Huang S, Wang J, Ahmad R, Liu B, Xu ZY (2018) Trithorax-group proteins ARABIDOPSIS TRITHORAX4 (ATX4) and ATX5 function in abscisic acid and dehydration stress responses. New Phytol **217**: 1582–1597

Lu F, Li G, Cui X, Liu C, Wang XJ, Cao X (2008) Comparative analysis of JmjC domain-containing proteins reveals the potential histone demethylases in Arabidopsis and rice. J Integr Plant Biol **50**: 886–896

Luger K, Dechassa ML, Tremethick DJ (2012) New insights into nucleosome and chromatin structure: an ordered state or a disordered affair? Nat Rev Mol Cell Biol **13**: 436–447

Luo YX, Hou XM, Zhang CJ, Tan LM, Shao CR, Lin RN, Su YN, Cai XW, Li L, Chen S (2020) A plant-specific SWR1 chromatin-remodeling complex couples histone H2A. Z deposition with nucleosome sliding. EMBO J **39**: e102008

Mizuguchi G, Shen X, Landry J, Wu WH, Sen S, Wu C (2004) ATP-driven exchange of histone H2AZ variant catalyzed by SWR1 chromatin remodeling complex. Science **303**: 343–348

Papamichos-Chronakis M, Watanabe S, Rando OJ, Peterson CL (2011) Global regulation of H2A. Z localization by the INO80 chromatin-remodeling enzyme is essential for genome integrity. Cell **144**: 200–213

Pien S, Fleury D, Mylne JS, Crevillen P, Inzé D, Avramova Z, Dean C, Grossniklaus U (2008) ARABIDOPSIS TRITHORAX1 dynamically regulates FLOWERING LOCUS C activation via histone 3 lysine 4 trimethylation. Plant Cell **20**: 580–588

Potok ME, Wang Y, Xu L, Zhong Z, Liu W, Feng S, Naranbaatar B, Rayatpisheh S, Wang Z, Wohlschlegel JA (2019) Arabidopsis SWR1-associated protein methyl-CpG-binding domain 9 is required for histone H2A. Z deposition. Nat Commun **10**: 1–14

Proveniers M, Rutjens B, Brand M, Smeekens S (2007) The Arabidopsis TALE homeobox gene ATH1 controls floral competency through positive regulation of FLC. Plant J **52**: 899–913

Ramirez F, Ryan DP, Gruning B, Bhardwaj V, Kilpert F, Richter AS, Heyne S, Dundar F, Manke T (2016) deepTools2: a next generation web server for deep-sequencing data analysis. Nucleic Acids Res **44**: W160–165

Robinson MD, McCarthy DJ, Smyth GK (2010) edgeR: a Bioconductor package for differential expression analysis of digital gene expression data. Bioinformatics **26**: 139–140

Sarnowska E, Gratkowska DM, Sacharowski SP, Cwiek P, Tohge T, Fernie AR, Siedlecki JA, Koncz C, Sarnowski TJ (2016) The role of SWI/SNF chromatin remodeling complexes in hormone cross-talk. Trends Plant Sci **21**: 594–608

Saze H, Shiraishi A, Miura A, Kakutani T (2008) Control of genic DNA methylation by a jmjC domain-containing protein in *Arabidopsis thaliana*. Science **319**: 462–465

Shi L, Sun L, Li Q, Liang J, Yu W, Yi X, Yang X, Li Y, Han X, Zhang Y (2011) Histone demethylase JMJD2B coordinates H3K4/H3K9 methylation and promotes hormonally responsive breast carcinogenesis. Proc Natl Acad Sci USA **108**: 7541–7546

Shilatifard A (2008) Molecular implementation and physiological roles for histone H3 lysine 4 (H3K4) methylation. Curr Opin Cell Biol **20**: 341–348

Sijacic P, Holder DH, Bajic M, Deal RB (2019) Methyl-CpG-binding domain 9 (MBD9) is required for H2A. Z incorporation into chromatin at a subset of H2A. Z-enriched regions in the Arabidopsis genome. PLoS Genet **15**: e1008326

Smith E, Lin C, Shilatifard A (2011) The super elongation complex (SEC) and MLL in development and disease. Genes Dev **25**: 661–672

Tan LM, Liu R, Gu BW, Zhang CJ, Luo J, Guo J, Wang Y, Chen L, Du X, Li S et al. (2020) Dual recognition of H3K4me3 and DNA by the ISWI component ARID5 regulates the floral transition in Arabidopsis. Plant Cell **32**: 2178–2195

Thompson JD, Higgins DG, Gibson TJ (1994) CLUSTAL W: improving the sensitivity of progressive multiple sequence alignment through sequence weighting, position-specific gap penalties and weight matrix choice. Nucleic Acids Res **22**: 4673–4680

Thorstensen T, Grini PE, Aalen RB (2011) SET domain proteins in plant development. Biochim Biophys Acta **1809**: 407–420

Wang J, Gao S, Peng X, Wu K, Yang S (2019) Roles of the INO80 and SWR1 chromatin remodeling complexes in plants. Int J Mol Sci **20**: 4591

Wang ZP, Xing HL, Dong L, Zhang HY, Han, CY, Wang XC, Chen QJ (2015) Egg cell-specific promoter-controlled CRISPR/Cas9 efficiently generates homozygous mutants for multiple target genes in Arabidopsis in a single generation. Genome Biol **16**: 144

Warnes GR, Bolker B, Bonebakker L, Gentleman R, Huber W, Liaw A, Lumley T, Maechler M, Magnusson A, Moeller S (2020) gplots: various R programming tools for plotting data. R package version 3.1.1. https://cran.r-project.org/web/packages/gplots/gplots.pdf, https://github.com/talgalili/gplots

Wickham H (2016) ggplot2: Elegant Graphics for Data Analysis, Berlin, Germany, Springer, p 224.

Yamane K, Toumazou C, Tsukada YI, Erdjument-Bromage H, Tempst P, Wong J, Zhang Y (2006) JHDM2A, a JmjC-containing H3K9 demethylase, facilitates transcription activation by androgen receptor. Cell **125**: 483–495

Yang C, Yin L, Xie F, Ma M, Huang S, Zeng Y, Shen WH, Dong A, Li L (2020) AtINO80 represses photomorphogenesis by modulating nucleosome density and H2A. Z incorporation in light-related genes. Proc Natl Acad Sci USA **117**: 33679–33688

Yao T, Song L, Jin J, Cai Y, Takahashi H, Swanson SK, Washburn MP, Florens L, Conaway RC, Cohen RE (2008) Distinct modes of regulation of the Uch37 deubiquitinating enzyme in the proteasome and in the Ino80 chromatin-remodeling complex. Mol Cell **31**: 909–917

Yu G, Wang LG, Han Y, He QY (2012) clusterProfiler: an R package for comparing biological themes among gene clusters. Omics **16**: 284–287

Zander M, Willige BC, He Y, Nguyen TA, Langford AE, Nehring R, Howell E, McGrath R, Bartlett A, Castanon R (2019) Epigenetic silencing of a multifunctional plant stress regulator. eLife **8**: e47835

Zang C, Schones DE, Zeng C, Cui K, Zhao K, Peng W (2009) A clustering approach for identification of enriched domains from histone modification ChIP-Seq data. Bioinformatics **25**: 1952–1958

Zhang C, Cao L, Rong L, An Z, Zhou W, Ma J, Shen WH, Zhu Y, Dong A (2015a) The chromatin-remodeling factor AtINO80 plays crucial roles in genome stability maintenance and in plant development. Plant J **82**: 655–668

Zhang S, Zhou B, Kang Y, Cui X, Liu A, Deleris A, Greenberg MV, Cui X, Qiu Q, Lu F (2015b) C-terminal domains of histone demethylase JMJ14 interact with a pair of NAC transcription factors to mediate specific chromatin association. Cell discovery **1**: 1–13

Zhang Y, Liu T, Meyer CA, Eeckhoute J, Johnson DS, Bernstein BE, Nusbaum C, Myers RM, Brown M, Li W (2008) Model-based analysis of ChIP-Seq (MACS). Genome Biol **9**: 1–9

Zhao QQ, Lin RN, Li L, Chen S, He XJ (2019) A methylated-DNA-binding complex required for plant development mediates transcriptional activation of promoter methylated genes. J Integr Plant Biol **61**: 120–139